The cell-surface 5′-nucleotidase CD73 defines a functional T memory cell subset that declines with age

Fengqin Fang[1,2,11], **Wenqiang Cao**[1,2,3,11], **Weikang Zhu**[4,5], **Nora Lam**[6,7], **Lingjie Li**[8,9], **Sadhana Gaddam**[8], **Yong Wang**[4,5], **Chulwoo Kim**[1,2], **Simon Lambert**[1,2], **Huimin Zhang**[1,2,3], **Bin Hu**[1,2], **Donna L. Farber**[7,10], **Cornelia M. Weyand**[1,2,3], **Jörg J. Goronzy**[1,2,3,12,*]

[1]Division of Immunology and Rheumatology, Department of Medicine, Stanford University, Stanford, CA, USA

[2]Department of Medicine, Palo Alto Veterans Administration Healthcare System, Palo Alto, CA, USA

[3]Department of Immunology, Mayo Clinic College of Medicine and Science, Rochester, MN, US

[4]CEMS, NCMIS, HCMS, MDIS, Academy of Mathematics & Systems Science, Chinese Academy of Sciences, Beijing 100190, China

[5]Center for Excellence in Animal Evolution and Genetics, Chinese Academy of Sciences, Kunming 650223, China

[6]Department of Pathology and Cell Biology, Columbia University Irving Medical Center, New York, NY 10032, USA

[7]Department of Microbiology and Immunology, Columbia University Irving Medical Center, New York, NY 10032, USA

[8]Program in Epithelial Biology and Department of Dermatology, Stanford University School of Medicine, Stanford, CA 94305, USA

[9]Department of Histoembryology, Genetics and Developmental Biology, Shanghai Jiao Tong University School of Medicine, Shanghai Key Laboratory of Reproductive Medicine, Shanghai 200025, China

[10]Department of Surgery, Columbia University Irving Medical Center, New York, NY 10032, USA

[11]These authors contributed equally

[12]Lead contact

[*]Correspondence: jgoronzy@stanford.edu.

DECLARATION OF INTERESTS
The authors declare no competing interests.

SUMMARY

Memory T cells exhibit considerable diversity that determines their ability to be protective. Here, we examine whether changes in T cell heterogeneity contribute to the age-associated failure of immune memory. By screening for age-dependent T cell-surface markers, we identify CD4 and CD8 memory T cell subsets that are unrelated to previously defined subsets of central and effector memory cells. Memory T cells expressing the ecto-5′-nucleotidase CD73 constitute a functionally distinct subset of memory T cells that declines with age. They resemble long-lived, polyfunctional memory cells but are also poised to display effector functions and to develop into cells resembling tissue-resident memory T cells (T_{RMs}). Upstream regulators of differential chromatin accessibility and transcriptomes include transcription factors that facilitate CD73 expression and regulate TRM differentiation. CD73 is not just a surrogate marker of these regulatory networks but is directly involved in T cell survival.

Graphical Abstract
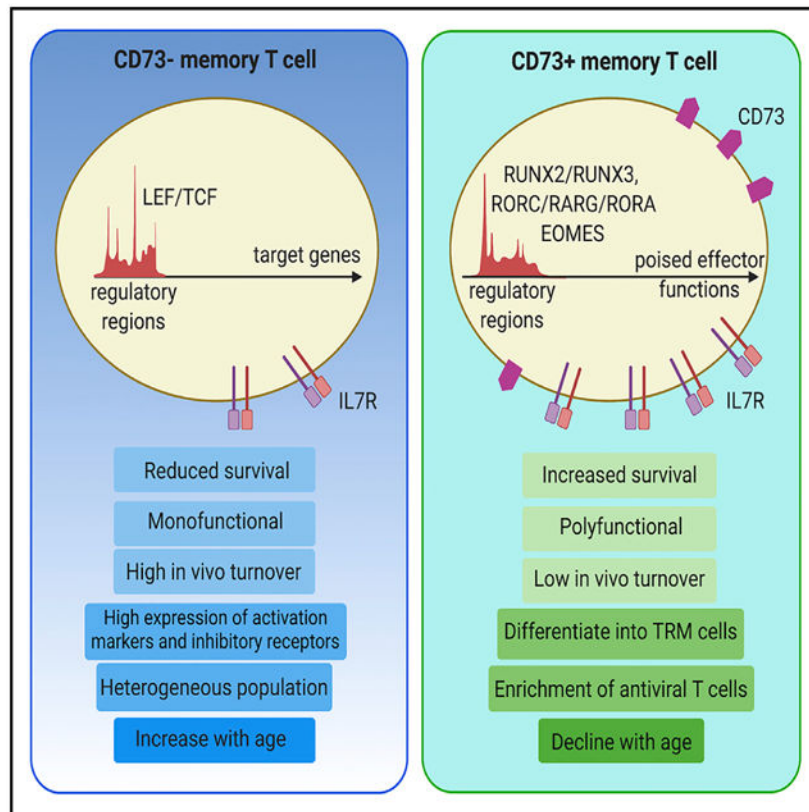
In brief

Fang et al. describe a subset of memory T cells that are long lived, highly functional, and have the ability to differentiate into tissue-residing cells. These cells are characterized by CD73 as a defining cell-surface marker. Decline of this population in older adults may contribute to failing T cell memory.

INTRODUCTION

Immune aging is associated with a decline in immune memory. A classic example is shingles, a reactivation of the varicella zoster virus (VZV) that affects up to 50% of the human population by the age of 80 years. Examples of recurring infections are pneumococcal disease and infections with the respiratory syncytial virus, both childhood infections with increased morbidity and mortality in the elderly. Moreover, T cell immunity does not provide protection against the annual influenza infections that occur due to antigenic drifts in antibody epitopes, although T cell epitopes appear to be relatively conserved (Koutsakos et al., 2019). Conversely, memory cell function to other pathogens can be lastingly effective. For example, symptomatic reactivation of EBV and CMV is rarely seen with normal aging. This dichotomy is also illustrated by the response to the live VZV vaccine Zostavax and the VZV component vaccine Shingrix that differ in their abilities to generate lasting immune memory in the elderly (Sadaoka and Mori, 2018).

Important functional domains for memory T cells are their durability, their ability to proliferate, their migration patterns, and their poised state to exert effector function. Cell-surface markers for conventional T cell subsets of central and effector memory (T_{CM}, T_{EM}) and of T_{EMRA} cells have been widely used to examine the influence of age on peripheral T cells. In general, the distribution of CD4 memory T cell subsets is relatively stable over adult life, while CD8 T_{EM} and T_{EMRA} populations accumulate. Studies of functional CD4 T cells based on their cytokine production patterns such as TH1, TH17, and TH2 T cells have not shown a consistent change with age. Distinct from T cells primed by exogenous pathogens, naive T cells may also acquire memory-like properties following self-antigen recognition during normal homeostasis, coined as "virtual" and "innate" memory T cells. Such virtual CD8 T cells accumulate with age. Whether they are as beneficial as normal memory cells in a recall response remains debated (White et al., 2017). They lack the clonal enrichment of antigen-specific T cells, a prerequisite of immune memory, but they also have a reduced proliferative potential in old individuals (Quinn et al., 2018).

Conventional markers incompletely define the heterogeneity of memory T cells. The recent progress in single-cell cytometric and RNA sequencing (RNA-seq) analysis has led to a plethora of cell-surface marker combinations defining memory cell subsets that only in part have been correlated with functional properties (Jameson and Masopust, 2009, 2018). To examine memory T cell heterogeneity with age, we probed a transcriptome dataset of human peripheral CD4 and CD8 T cell subsets from young and old adults for cell-surface markers that changed with age (accession code: SRA: PRJNA638216). We identified CD73 as a molecule that allowed a hereto-unknown subsetting of memory CD4 and CD8 T cells that does not correlate with previously defined subsets, is functionally meaningful, and changes with age. CD73+ memory T cells excel in their durability, poised effector function, and ability to differentiate into cells reminiscent of T_{RM} *in vitro* under TCR and subsequent transforming growth factor (TGF)-β/interleukin (IL)-15 stimulation. Transcription factor (TF) networks that are important for memory cell function regulate transcription of CD73 that therefore identifies a selective differentiation state. Equally importantly, CD73 directly confers survival advantage in murine antiviral responses. Unlike CD73+ T cells, CD73−

memory CD4 T cells are a heterogeneous population that increases with age and includes actively replicating, short-lived cells largely devoid of polyfunctional T cells.

RESULTS

Age-associated changes in memory T cell heterogeneity

In RNA-seq studies of peripheral T cell subsets, we found that the expression of *NT5E* encoding the 5′-nucleotidase CD73 declined with age. Consistent with these results, we found a decline of CD73$^+$ cells in total CD4 or CD8 T cells from 24 old compared to 28 young individuals (Figures 1A and 1C). To examine the relationship of CD73 expression to conventional T cell subset definitions, we compared peripheral blood mononuclear cells (PBMCs) from fourteen 20- to 35- and twelve 65- to 80-year-old healthy adults. CD73 was expressed on all CD4 and CD8 T cell subsets (Figure S1A). For CD4 cells, expression was more frequent in naive and T_{EMRA} cells with 25% each compared to 15% in T_{CM} (Figure 1B). Expression of CD73 in CD8 T cell subsets was generally higher, with most naive and close to 40% of T_{CM} and T_{EM} CD8 T cells expressing CD73 (Figure 1D). Importantly, CD73 expression did not correlate with the expression of chemokine receptors that are generally used to subset memory T cells. For all CD4 and CD8 T cell subsets, except CD8 T_{CM}, expression of CD73 significantly decreased with age (Figures 1B and 1D). This decline was a loss in cells; cell-surface expression of CD73 on gated CD73$^+$ cells did not change with age in naive or memory CD4 or memory CD8 subsets (Figure S1B). An age-related change in naive CD8 T cells may reflect the change in composition of this subset with age.

CD73$^+$ CD4$^+$ T cells display a transcriptome of superior effector as well as memory cell function

To identify functional differences, we sorted human CD73$^+$ and CD73$^-$ memory CD4 T cells from three young adults for RNA-seq. 634 genes were upregulated in the CD73$^+$ subset, while 594 genes were downregulated as shown in the volcano plot in Figure 1E with selected genes highlighted. Genes that were more highly expressed in CD73$^+$ T cells included genes characteristic of effector T cells, such as *RUNX3*, *RORC*, *PRDM1*, *STAT4*, *TBX21*, *IL12R*, *IL23R*, and *CXCR3* (Weng et al., 2012). In parallel, selected genes pertaining to long-lived memory T cells such as *IL7R*, *EOMES* (Banerjee et al., 2010), *RUNX2* (Hu and Chen, 2013; Olesin et al., 2018), *ABCB1* (*MDR1*), and *CD161* (*KLRB1*) (Alsuliman et al., 2017) were also more highly expressed. Moreover, expression of *BHLHE40* critical to maintaining fitness and functionality of T_{RM} and tissue-infiltrating T cells was increased (Li et al., 2019; Park and Mackay, 2019). c-KIT, also overexpressed in CD73$^+$ T cells, is a survival factor that so far has not been implicated in memory cell longevity. The differential gene expression was not due to unequal representation of T_{CM} and T_{EM} in CD73$^+$ and CD73$^-$ subsets. Although the distributions were significantly different, T_{CM} were dominant in both subsets and the absolute differences were small (Figure S1C). To further examine the relationship of CD73$^+$ cells to T_{CM} or T_{EM} cells, we retrieved RNA-seq data from the NCBI database (GEO: GSE97863) comparing human T_{CM} and T_{EM} cells (Tian et al., 2017). We did not find a correlation of the differences between CD73$^+$ and CD73$^-$ cells with those between T_{CM} and T_{EM} cells, supporting the notion that

subsetting memory CD4 T cells based on CD73 expression is distinct from traditional T_{CM} and T_{EM} cells (Figure 1F).

GO term analysis, using the DAVID Bioinformatics tool, yielded a significant enrichment in CD73$^+$ cells for "positive regulation of interferon (IFN)-γ production," "inflammatory response," "response to virus," and "positive regulation of cell migration" (Figure 2A). Gene set enrichment analysis (GSEA) confirmed the correlation with inflammatory response gene expression (Figure 2B). Moreover, a strong correlation of CD73 positivity was found with ribosomal gene expression (Figure 2B), reminiscent of the increased ribosomal activity in antigen-stimulated effector CD8 T cells that has been implicated in memory-fate decisions (Araki et al., 2017). Further analysis of the transcriptome data showed that CD73$^+$ and CD73$^-$ memory T cells, although almost equally represented in central and effector memory T cells, exhibited different propensities in migratory patterns (Figure S2A). CD73$^+$ cells have decreased expression of *CCR3*, *CCR4*, *CCR7*, *CCR8*, and *CXCR5* but increased transcription of *CCR2*, *CCR6*, *CCR9*, *CXCR3*, *CXCR4* and *CXCR6*, a pattern that enables cells to migrate to peripheral tissues (Kim et al., 2001; Olive et al., 2011; Wang et al., 2009). Moreover, the two subsets differed in the expression of CD4 sub-lineage-defining genes (Duhen et al., 2014). CD73$^+$ cells exhibited TH1, TH17, and TH1.17 gene patterns, while Treg and Th2 signatures were found in CD73$^-$ T cells (Figure S2B). However, both CD73$^+$ and CD73$^-$ T cells were diverse populations, each including different lineages. For example, Tregs defined by FOXP3 expression accounted only for a minority of less than 15% of CD73$^-$ memory T cells (Figure S2C).

To compare functional properties of CD73$^+$ and CD73$^-$ memory T cells, we tested their response to activation signals. CD69 was more readily induced in CD73$^+$ cells upon CD3/CD28 triggering, indicating a greater responsiveness of this subset to TCR stimulation (Figure 2C). Intracellular cytokine staining upon ionomycin and PMA stimulation showed higher frequencies of CD73$^+$ memory CD4 T cells that were poised to secrete IL-2, TNF-α, IFN-γ, and/or IL-17A and fewer producers of IL-21 and IL-4 (Figure 2D). In addition, based on the MFI in the gated cytokine-positive population, the amount of IL-2, TNF-α, and IFN-γ produced per cell was higher (Figure S2D). Similarly, CD73$^+$ memory CD8 T cells generated more TNF-α per cell and were more frequently able to produce IL-2, IFN-γ, and granzyme B compared to CD73$^-$ cells (Figure 2E; Figure S2E). Up to 30% of CD73$^+$ memory CD4 T cells secreted all three cytokines tested (IFN-γ, IL-2, and TNF-α) compared to 13% of CD73$^-$ cells after 6 h of anti-CD3/CD28 stimulation (Figure 2F). In contrast, the percentage of cells secreting none or only one cytokine was significantly higher in CD73$^-$ memory CD4 T cells. A similar bias for polyfunctionality (here defined as the coproduction of IL-2, IFN-γ, and granzyme B) was observed for CD8 memory T cells (Figure 2F). The superior effector function of CD73$^+$ T cells was not due to a higher frequency of T_{EM} cells; we compared cytokine production of CD73$^+$ and CD73$^-$ cells in gated T_{CM} and T_{EM} subsets and saw similar patterns (Figure S2F).

Resistance of CD73$^+$ T cells to undergo cell death

While CD73$^+$ memory T cells had superior effector function, transcriptome analysis also indicated an increased expression of growth factor receptors and survival factors, unlike

short-lived effector T cells (Figure 1E). qRT-PCR assays confirmed the elevated expression of *BCL2*, *IL7R*, and *KIT* by CD73^{+} cells (Figure 3A). *In vitro* culture in the absence of cytokines showed a 3-fold higher propensity of CD73^{−} T cells to undergo apoptosis (Figure 3B). Differential expression of the IL7R receptor on CD73^{+} T cells was consistent for the T_{CM}, T_{EM}, and T_{EMRA} subsets of CD4 and CD8 memory T cells (Figures 3C and 3D). It is noteworthy that, with the exception of CD8 T_{EMRA} cells and a subset of CD8 T_{EM} cells, IL-7R was still detectable on CD73^{−} cells but clearly reduced on a per cell basis. *In vitro* culture in the presence of IL-7 showed that both populations increased their survival rate (Figure 3E; Figure S3A). CD117 encoded by *c-KIT* was expressed on a small subset of CD73^{+} CD4 and CD8 memory T cells (Figure S3B). Given the small population size, culture with stem cell factor (SCF) treatment did not provide a global, detectable survival benefit (Figure S3C). c-KIT expression declined with age in T_{CM} and T_{EM} subsets of CD4 and CD8 T cells (Figure S3D).

CD73^{−} memory CD4 T cells are a high-turnover population with limited effector function

CD73^{−} T cells represent the majority of central and effector memory CD4 T cells, but their transcriptome suggested an inferior effector function. DAVID GO term analysis of the CD73^{−} cell transcriptome was enriched for the terms of "cell division" and "regulation of cell cycle" as well as "MHC class II molecules" (Figure S4A). Consistent with the DAVID analysis, GSEA showed a high correlation with the hallmark categories of "E2F targets" and "mitotic spindle" as well as with two widely used gene sets distinguishing quiescent and dividing cells (Graham et al., 2007) (Figure S4B).

To obtain further evidence for high *in vivo* turnover, we determined *ex vivo* expression of Ki67, that is restricted to actively and recently cycling cells (De Boer and Perelson, 2013). *MKI67* mRNA was almost undetectable in CD73^{+} and clearly elevated in CD73^{−} CD4 T cells (Figure S4C). Flow cytometry detected around 4% of Ki67^{+} cells in CD73^{−} CD4 memory T cells compared to less than 2% in CD73^{+} cells (Figure S4D). The difference in cycling cells was not due to an irreversible defect; the proliferative response to anti-CD3/CD28 Ab activation was nearly equal between the two subsets (Figure S4E).

CD73^{+} and CD73^{−} memory T cells are governed by distinct transcriptional regulatory networks

Transcriptional profiling of transcription factors that define T cell differentiation states showed that CD73^{+} T cells have increased expression of effector (including RORC, PRDM1, RUNX3, and TBX21) as well as memory cell-determining TFs (including RUNX2, EOMES, and BHLHE40) compared to CD73^{−} cells (Figure 4A). To further define TF networks involved in determining the distinct differentiation states, we compared chromatin accessibilities of CD73^{+} and CD73^{−} memory T cells by ATAC sequencing (ATAC-seq). Accessibility maps differed greatly, with 3,961 sites significantly more open and 2,209 sites more closed in CD73^{+} cells (Figure 4B). DNA was completely inaccessible at the *NT5E* locus in CD73^{−} T cells while accessibility to *CXCR5* was increased, consistent with the transcriptional data (Figure 4C).

HOMER analysis of differentially accessible union peaks yielded a highly significant enrichment for RUNT (RUNX2, RUNX3), NR (RORC, RORA, RARG), and T-box family (EOMES, T-bet) TF motifs in CD73+ cells, while HMG family TFs (LEF1, TCF1) were the only motif enriched in CD73− cells (Figure 4D). We integrated the differences in transcriptomes and in chromatin accessibilities with public chromatin immunoprecipitation sequencing (ChIP-seq) and T cell-specific chromatin interaction data using TF-regulatory region-target gene triplet inference modeling to construct the signature networks of key TFs and their target genes for the two T cell subsets (Duren et al., 2017; Lai et al., 2018) (Figure S5A). The center of the major network of CD73+ T cells was formed by RUNX2 and RUNX3, while one smaller network was centered on EOMES, both of them indicative of CD73+ T cells being long-term memory T cells (Hu and Chen, 2013; Olesin et al., 2018) (Figure 5A). Flow cytometric studies confirmed increased expression of RUNX2 and RUNX3 in CD73+ versus CD73− T cells, irrespective of whether they were T_{CM} or T_{EM} (Figure S5B).

NT5E (encoding CD73) was the target gene with most significant inference, additional target genes included *ADAM23*, *MATK*, *CFH*, and *ITGA1*. RUNX2 silencing and overexpression confirmed its role in controlling NT5E transcription in CD4 as well as CD8 T cells (Figures 5B and 5C). RUNX3 silencing did not have an effect on CD73 expression (Figure 5D); however, forced overexpression upregulated NT5E transcription (Figure 5E). Additional clusters were centered on RORC/RARG and ETS2. RORC in mature T cells is pivotal for induction and maintenance of TH17 effector T cells. The retinoic acid receptor encoded by RARG promotes the differentiation and homing of gut-resident memory CD8 T cells (Iwata et al., 2004; Reis et al., 2013). Thus, CD73 expression is a biomarker of a unique constellation of TFs in these cells. However, none of these TFs changes with age. Thus, the diminution of CD73+ T cells is not just a reflection of the regulation of CD73 expression but is a true decline in a functional T cell subset.

In contrast to CD73+ T cells, the major network in CD73− T cells centered on HMG family TFs including LEF1, TCF3, and TCF7 that are known to be important for stem-like memory T cells (Figure 5A). A second smaller cluster centered around several TFs that share the functional property of being involved in dampening T cell effector functions. These genes include the transcriptional repressors TGIF2 and ZEB1, several members of the KLF family and FOXO1. These patterns were unexpected for cells that appear to be under increased turnover. A third cluster centered around CTCF together with the cohesion components RAD21 and SMC3, possibly indicating differences in chromatin structural maintenance related to the increased mitotic activity of CD73− T cells.

CD73+ memory T cells are prone to differentiate into cells expressing a tissue-resident memory phenotype

Among TFs differentially expressed or identified in the network analysis for CD73+ cells, at least four were described as critical for T_{RM} cell differentiation, function, or survival, including PRDM1 (Mackay et al., 2016), RUNX3 (Milner and Goldrath, 2018; Milner et al., 2017), BHLHE40 ((Li et al., 2019); Park and Mackay, 2019), and RORC (Amezcua Vesely et al., 2019). To examine whether CD73+ and CD73− memory T cells have equal

potential to differentiate into T_{RM} cells, we cultured freshly isolated human memory T cells under sequential TCR and TGF-β/IL-15 stimulation (Reis et al., 2013; Zhang and Bevan, 2013). CD73 expression was relatively stable under these tissue culture condition, in particular, CD73 expression was not induced in sorted CD73$^-$ T cells, indicating that CD73$^+$ T cells in the T_{RM} population do not derive from CD73$^-$ memory cells (Figure S6A). After differentiation, CD73$^+$ cells had elevated cell-surface expression of T_{RM} markers compared to CD73$^-$ cells (Figures 6A and 6B; Figures S6B and S6C). For CD4 CD73$^+$ T cells, the combination of CD69 and CXCR6 was the most frequent phenotype. For CD8$^+$ CD73$^+$ cells, the T_{RM}-associated marker combinations CD69$^+$CXCR6$^+$ and CD69$^+$CD103$^+$ were about equally frequent. Conversely, CD73 expression was frequent on CD69$^+$CXCR6$^+$ cells, while infrequent on CD69$^-$CXCR6$^-$ cells (Figure S6D).

The key TFs regulating CD73 expression, RUNX2 and RUNX3, were also supporting the expression of T_{RM} markers. RUNX2 silencing during T_{RM} generation reduced the gain in CD103 expression, while keeping CD69 expression unaffected (Figure 6C; Figure S6E). The forced expression of RUNX2 upregulated both CD103 and CD69 (Figure 6D; Figure S6F) in addition to CXCR6 (Figure S6G). RUNX3 silencing (Figure 6E; Figure S6H) as well as overexpression (Figure 6F; Figure S6I) documented a role for RUNX3 in CD69 and less so for CD103 expression.

We compared the two subsets of CXCR6$^+$CD69$^+$ and CXCR6$^-$CD69$^-$ cells differing in CD73 for the expression of 19 T_{RM} core genes (Kumar et al., 2017; Milner and Goldrath, 2018; Schenkel and Masopust, 2014). Three genes were hardly detectable; all other 16 genes were consistent with the pattern described as a T_{RM} profile. *S1PR1*, *KLF2*, *KLF3*, *SELL*, *CCR7*, and *TCF1* promoting tissue exit were decreased in CXCR6$^+$CD69$^+$ cells (Figure 6G); *CXCR6*, *CD69*, and *ITGA1* with roles in tissue homing and retention, *RUNX3*, *BHLHE40*, *PRDM1*, *RORC* being crucial for T_{RM} differentiation and function, *BCL2* for cell survival, and the inhibitory molecules *PDCD1* and *DUSP6* were all increased in CD69$^+$CXCR6$^+$ cells (Figure 6G). To control for changes in CD73 expression in the T_{RM} differentiation culture, we sorted CD73$^+$ and CD73$^-$ memory T cells before sequentially culturing them with TCR and then TGF-β signaling (Figure S7). The CD73 marker was preserved before and after cell differentiation (Figure S6A). Consistent with data shown in Figures 6A and 6B, CD69, CXCR6, and CD103 T_{RM} markers were significantly elevated in CD73$^+$ compared to CD73$^-$ cells (Figures S7A and S7B). Moreover, compared to CD73$^-$ cells, the expression profile of 11–12 T_{RM} signature genes in CD73$^+$ cells was consistent with T_{RM} features with upregulation of tissue homing and retention molecules (e.g., *CD49a*, *CRTAM*, *CD69*, and *CXCR6* as well as additional CD101 and CD103 for CD8 T cells) and downregulation of genes involved in tissue exiting (e.g., *CX3CR1*, *KLF2*, *KLF3*, *S1PR1*, *S1PR5*, and *SELL*, Figures S7C and S7D).

As shown in Figure 1, the size of the CD73$^+$ memory cell compartment declines with age. If T_{RM}s derive from CD73$^+$ T cells, the loss in CD73$^+$ T cells should result in a lesser generation of T_{RM}s with age. T_{RM}s were generated *in vitro* from memory cells of adults younger than 35 years or older than 65 years as described above. After differentiation, old adults continued to have fewer CD73$^+$ T cells in the CD4 as well as the CD8 T cell subset (Figures 6H and 6I). Generation of T_{RM}s was reduced in parallel. CD69$^+$CXCR6$^+$ cells were

around 5% for young compared to less than 3% for old memory CD4 T cells (Figure 6H). Similarly, the frequency of CD103$^+$ cells was higher for memory CD8 T cells from young than from old adults (Figure 6I). Frequencies of CD73$^+$ cells highly correlated with those of CD69$^+$CXCR6$^+$ cells in CD4 T cells and with CD103$^+$ cells in CD8 T cells (Figures 6J and 6K). Taken together, the lower frequencies of CD73$^+$ cells accounted for reduced *in vitro* T$_{RM}$ generation with age.

CD73 influences T cell survival and T$_{RM}$ differentiation *in vivo*

To examine whether T$_{RM}$ in human tissues are characterized by the expression of CD73, we collected spleen, lung, and jejunum tissues from three organ donors older than 65 years (Figure 7A). CD73 expression on CD4 T cells was very low in two of the three spleens (Figure 7A). Spleens from all three donors had a CD8 T cell subpopulation with high expression of CD73; two had an additional CD73^{low} population. Virtually the entire CD73^{hi} subpopulation co-expressed CD103 and CD69. Compared to splenic T cells, CD73-expressing T cells were enriched in the jejunum, especially for CD8 T cells. Up to 25% of CD45RA$^-$CD4$^+$ and up to 77% of CD45RA$^-$CD8$^+$ T cells expressed CD73. CD73$^+$ T cells frequently expressed CD103, in particular jejunal CD8 T cells, while virtually all jejunum cells expressed CD69. CD73 expression was infrequent in lung T cells, but when present, correlated with CD69 and CD103 expression.

To explore the mechanistic relationship between CD73 and memory T cell survival and tissue residency of T$_{RMs}$, we used the LCMV infection mouse model. At the effector stage on day 8 after LCMV infection, IA^{b}GP66 tetramer$^+$ spleen CD4 T cells varied highly in CD73 expression with about 50% of antigen-specific CD4 T cells being CD73-positive (Figure 7B). In contrast, the majority of LCMV-specific CD4 T cells at the memory stage on day 85 expressed CD73 (Figure 7B). LCMV IA^{b}GP61 tetramer-specific CD4 T cells from lung and liver tissue also highly expressed CD73 (Figure 7C).

Similarly, human peripheral blood CD8 T cells specific to viral antigens are enriched in the CD73$^+$ memory subset (Figure 7D). We recruited HLA-A2 donors of different ages and compared CD8 T cells specific to the EBV BMLF1 and the influenza M1 proteins. We gated on tetramer-positive cells within the CD45RO$^+$ and CD45RO$^-$CD62L$^-$ CD8$^+$ memory T cell population and determined the frequency of CD73 expression. CD73 expression was found to be highly enriched in antigen-specific memory T cells. Significantly more CD8 T cells specific for the HLA-A2 GILGFVFTL influenza tetramer expressed CD73 than the bulk population. A loss in CD73 expression for influenza matrix-specific T cells with age was only observed in few individuals. Similar results were obtained for CD8 T cells specific for BMLF1; BMLF1-specific T cells mostly expressed CD73, almost irrespective of age (Figure 7D). Taken together, CD73 identifies a memory T cell subset that is enriched for virus-specific T cells, indicating the longevity of this population.

To determine whether CD73 is a surrogate marker or whether it is directly involved in T$_{RM}$ differentiation and memory T cell survival, we used an adoptive transfer system and LCMV infection. CD45 congenic SMARTA cells were retrovirally transduced with control or *NT5E* short hairpin RNA (shRNA). Successfully transduced cells expressing AmCyan were sorted and mixed at a ratio of 1:1 before injecting into the tail vein. Mice were then

infected with LCMV. On day 20 after infection, spleen, lung, and liver were analyzed for the relative percentage of each population (CD73KD versus WT cells) as well as their respective phenotypes (Figure 7E). WT cells were highly enriched compared to CD73KD cells in all three tissues, indicating improved survival. Moreover, WT cells in all three tissues expressed more CXCR6 and CD69 comparing to CD73KD cells, indicating that CD73 has direct role of CD73 in T_{RM} differentiation (Figure 7E).

DISCUSSION

Here, we describe that CD73 expression distinguishes two subsets of memory T cells with markedly different chromatin accessibility and transcriptional profiles that do not correlate with the conventional subset distinctions. CD73 is expressed on 10%–40% of cells within each of the CD4 and CD8 central and effector memory T cell subsets. CD73$^+$ T cells have many of the features that are associated with long-lived memory T cells including the expression of survival factors and the IL-7 receptor. In parallel, they are poised to express effector molecules upon restimulation, and they differentiate into cells with the marker profile of tissue-resident memory T cells.

The distinction of CD73$^+$ from CD73$^-$ T cells was primarily determined by a TF network that, among other genes, regulates transcription of *NT5E* encoding for CD73. We identified distinct TF—regulatory element—target gene triplet inference networks in the two subsets of memory cells using a recently described approach (Duren et al., 2017). A core group of TFs, topped by RUNX2 and RUNX3, was characteristic for CD73$^+$ T cells when compared to CD73$^-$ T cells and was involved in the transcriptional regulation of *NT5E* (p < 10^{-53} for enrichment). Silencing and overexpression experiments confirmed the dominant role of RUNX2 and to a lesser extent of RUNX3 in controlling *NT5E* transcription (Figure 5). Additional networks centered on EOMES that was also predicted to regulate *NT5E*, and members of the NR family, such as RARG and RORC, consistent with the notion that CD73$^+$ T cells are prone to express inflammatory cytokines. A fourth cluster of target genes centered on the TFs FLI1, ETS2 and THRA, again predicted transcriptional regulators of *NT5E*, suggesting that CD73 expression is a reflection of the TF networks that control this subset of memory T cells.

Compared to CD73$^-$ T cells, CD73$^+$ T cells have a survival advantage, possibly due to the increased expression of the anti-apoptotic gene BCL2 and several growth factor receptors. Previous studies have identified CD73$^+$ T cells as a chemotherapy-resistant population with upregulation of the aldehyde dehydrogenase 1 (ALDH1) activity (Murata et al., 2016). Consistent with this finding, we found ALDH1B1 and the drug-resistance gene ABCB1 both enriched in the transcriptome of CD73$^+$ cells (Figure 1E), which may contribute to increased cell survival. However, CD73 also supported survival directly as shown in knockdown experiments of antigen-specific cells after LCMV infection. CD73 converts AMP to adenosine that then triggers adenosine receptors, a mechanism that has been implicated in the negative regulatory function of Treg (Allard et al., 2017). Clearly, the population described here are not bona fide Tregs. In contrast to murine studies, co-expression of CD39 (cleaving ATP to AMP) and CD73 (generating adenosine from AMP) rarely exists in human T cells, indicating species-specific differences in Treg physiology.

How the supporting effect of CD73 on survival and T_{RM} generation observed here is related to the generation of adenosine is undetermined. Different adenosine receptors exist that can transmit positive or negative signals. The main adenosine receptor expressed on T cells is the negative regulatory G protein-coupled A2AR, consistent with adenosine inducing cell inhibition (Allard et al., 2017) or cell death in CD39-expressing short-lived effector T cells (Fang et al., 2016). However, it is possible that, dependent on the setting, A2AR stimulation can be beneficial for T cell function and survival. Stimulation of the A2AR activates PKA directing T cell differentiation (Cao et al., 2020), protecting T cells from activation-induced cell death (Himer et al., 2010) and preventing CD73+ T cells from cycling, thereby inducing quiescence (Hirata et al., 2018). Also, adenosine production in the tumor environment, generally considered immunosuppressive, has been shown to also support anti-tumor responses, probably by maintaining IL-7R expression and improving T cell survival (Cekic and Linden, 2014). Rosemblatt et al. (2021) have shown that adenosine supports homeostatic proliferation in a lymphopenic environment through upregulation of IL-7R, while inducing cell death in antigen-specific responses through inhibiting IL-2R and BCL2. Finally, CD73 may protect T cells by cleaving AMP and preventing stimulation of P1 receptors (Rittiner et al., 2012; Saze et al., 2013), while the generated adenosine is deaminated by adenosine deaminase (ADA) recruited by CD26. The expression of CD26 on CD73+ memory CD4 T cells is much higher than on CD73− cells.

Functionally, CD73+ T cells displayed properties that are expected from long-lived memory cells. Their decline with age therefore could explain the defect in immune memory. CD73+ memory T cells have a significantly lower turnover *in vivo* than CD73− memory T cells. *In vitro*, they are more resistant to undergo apoptosis, presumably due to increased BCL2 and IL-7R expression. They exhibit increased chromatin accessibility to regulatory regions of effector genes, consistent with the previous report that memory cells display the epigenetic signature of effector T cells based on DNA methylation and ATAC-seq studies (Akondy et al., 2017). Upon restimulation, they proliferate and efficiently produce inflammatory cytokines, frequently in combination with IL-2 attesting to their polyfunctionality. Many of these features are reminiscent of stem-like memory T cells that are regulated by TCF1 cells (Gattinoni et al., 2009). It was therefore surprising to see that more accessible regulatory regions in CD73+ CD4 T cells were not enriched for TCF binding motifs; on the contrary, we found a motif enrichment of TCF1 and even more so LEF1 at sites more accessible in CD73− T cells. We also saw increased expression of ribosomal genes in CD73+ T cells indicative of increased protein synthesis that is more characteristic of effector rather than memory cells. Subsetting memory T cells based on their CD73 expression therefore bears no relationship to the distinction between central or stem-like memory and effector memory T cells.

TF networks in CD73+ T cells, including the central position of RUNX3 and RORC, indicated a relationship to tissue-resident effector T cells. Indeed, CD73+ memory T cells were prone to differentiate *in vitro* upon TCR and subsequent TGF-β/IL-15 stimulation into T cells expressing phenotypic markers of T_{RMs}. CD4+CD73+ T cells differentiated into CD69+CXCR6+ T cells, which have a gene-expression profile similar to T_{RM} cells (Kumar et al., 2017; Milner and Goldrath, 2018; Schenkel and Masopust, 2014); CD8+CD73+ T cells acquired the classic CD69+CD103+ T_{RM} phenotype. Thus, CD73 appears to identify

a subset of circulating cells that is prone to differentiate into T_{RM} cells, possibly based on their TF networks. *In vivo* studies supported this interpretation. In T cells harvested from human tissue, CD103 expression was increased within the $CD73^+$ T cell population, in particular for CD8 T cells from the jejunum. In general, T_{RMs} are thought to derive from short-lived effector T cells that migrate to peripheral tissue sites and stay there permanently. However, T_{RMs} are also replenished from a pool of recirculating memory T cells (Ely et al., 2006; Enamorado et al., 2017; Slütter et al., 2017). Experiments in the mouse have characterized the recirculating CD8 population as intermediate positive for CX3CR1, while the corresponding CD4 population is undefined (Böttcher et al., 2015; Gerlach et al., 2016). Our data suggest that the $CD73^+$ T cell subsets of CD4 as well as CD8 T cells are highly enriched for cells able to express a T_{RM} phenotype.

Compared to $CD73^+$ cells, $CD73^-$ memory CD4 T cells are a more heterogeneous population, negatively defined as the absence of CD73. Transcriptome analysis suggested that they included regulatory T cells and TH2 and T follicular helper cells. Flow cytometry confirmed the enrichment for these populations but left a large fraction of the $CD73^-$ population unassigned (Figure 2; Figure S2C). Accordingly, TF networks did not center on lineage-specific transcription factors, but on the TCF/LEF family. However, in stark contrast to naive and stem-like memory cells that are generally regulated by TCF/LEF, functional enrichment analysis as well as GSEA of the transcriptome provided evidence for activation and high *in vivo* turnover of the $CD73^-$ population. Moreover, *in vitro* assays showed a shortened survival time, even in the presence of cytokines. These features are reminiscent of memory phenotype (T_{MP}) cells that are triggered by self-antigen (Kawabe et al., 2017; Miller et al., 2020) or commensal organisms. T_{MP} cells undergo a 2- to 3-fold faster turnover rate than do antigen-specific memory CD4 T cells (Seddon et al., 2003; Surh and Sprent, 2008; Younes et al., 2011). Their homeostatic proliferation depends on MHC recognition and TCR signaling rather than cytokine alone (Purton et al., 2007). Gossel et al. (2017) described a subset of memory T cells constantly replenished from naive T cells, which may represent T_{MP}. These newly generated memory cells expressed higher level of Ki67 than previously established memory cells, indicating rapid turnover.

Similar to T_{MP}, virtual memory (T_{VM}) cells are generated independent of the recognition of exogenous antigen, however, mostly only from naive CD8 T cells. CD8 T_{VM} cells have poor TCR-induced IFN-γ production comparing to true memory (T_{TM}) T cells (Haluszczak et al., 2009; Lee et al., 2013). Quinn et al. (2018) showed that CD8 T_{VM} cells are mostly mono-functional. Similarly, $CD73^-$ memory T cells produce less IFN-γ, and the majority of cells are mono-functional (Figure 2). Transcriptional profiling also showed elevated expression of IL-15Rβ in $CD73^-$ memory CD4 T cells. IL-15 signaling is known to play a pivotal role in T_{VM} cell generation (Sosinowski et al., 2013; White et al., 2016), and high expression of IL-15Rβ (CD122) has been considered a marker for T_{VM} cells. The proportion of T_{VM} cells in the mouse increases with age as does the fraction of $CD73^-$ T cells in humans as reported here.

Limitations of the study

In summary, we have identified a cell-surface marker, CD73 that defines a subset of memory T cells that are long lived, highly functional, and have the ability to differentiate into tissue-residing cells. This population is declining with age, but we do not know the mechanisms that causes this decline. A better understanding here is needed to develop interventions that prevent this decline. Based on the *in vitro* characterization of CD73$^+$ T cells and the finding that they are enriched for virus-specific T cells, we propose that this decline accounts for defective antiviral memory responses in older adults. Further *in vivo* and population studies are needed to validate this claim. Finally, CD73 may not only be a useful biomarker for developing strategies of better memory cell induction. We provide evidence that CD73 is directly important in T cell survival and T$_{RM}$ differentiation *in vivo* and propose a model of possible mechanisms that needs to be further developed.

STAR★METHODS

RESOURCE AVAILABILITY

Lead contact—Further information and requests for resources and reagents should be directed to and will be fulfilled by the Lead Contact, Dr. Jorg J. Goronzy (jgoronzy@stanford.edu).

Materials availability—This study did not generate new unique reagents except plasmid pLMPd-Amt Vector with Nt5e shRNAmir. A completed Materials Transfer Agreement may be required.

Data and code availability

- This paper does not report original code.

- RNA-seq data of CD4 and CD8 T cell subsets from young and old adults are available in SRA with accession code PRJNA638216. RNA- and ATAC-sequence data from CD73$^+$ and CD73$^-$ CD4 memory T cells were deposited in GEO under accession number GSE157164.

- Any additional information required to reanalyze the data reported in this paper is available from the lead contact upon request.

EXPERIMENTAL MODEL AND SUBJECT DETAILS

Study population and cells—De-identified leukocyte samples from 134 blood or platelet donors younger than 35 years or older than 65 years were purchased from Stanford University Blood bank. In addition, PBMCs were obtained from 11 healthy volunteers. 8 of these individuals were younger than 35 years old. Human tissues (spleen, lung and jejunum) were procured from three organ donors older than 65 years through collaboration with LiveOnNY, the organ procurement organization for the New York metropolitan area. The studies were approved by the Stanford University Institutional Review Board, and participants gave informed written consent. As confirmed by the Columbia University IRB, use of tissue samples obtained from brain-dead (deceased) individuals does not qualify as "human subjects" research.

Untouched total T or isolated CD4+ or CD8+ T cells were purified from buffy coats or whole blood with RosetteSep Human T or CD4+ or CD8+ T cell enrichment cocktails (STEMCELL Technologies, Cat#: 15061, 15062, 15063). Memory CD4+ or CD8+ T cells were either isolated from PBMCs by EasySep Human Memory CD4+ or CD8+ T cell enrichment kit (STEMCELL Technologies, Cat#: 19157 or 19159), or isolated from purified CD4+ or CD8+ T cells by CD45RO microbeads (see STAR methods). PBMCs were obtained by density gradient centrifugation using Lymphoprep (STEMCELL Technologies, Cat#: 07861). Purity of isolated cells was > 90%. Human spleen, lung and intestinal samples were processed using enzymatic and mechanical dispersion to generate single-cell suspensions containing high yields of live leukocytes.

Murine LCMV model—C57BL/6J (B6) mice were purchased from the Jackson Laboratory. LCMV-Armstrong was grown in BHK cells and titered in Vero cells. Male mice, 8–10 weeks of age, were adoptively reconstituted with transduced SMARTA cells and infected i.p. with a dose of 2×10^5 plaque-forming units (PFU). Retroviral transduction was performed as follows: *Nt5e* shRNAmir (CAGGTTGAGTTTGATGATAAAG) was inserted into pLMPd-Amt vector. Virions were packaged in the Plat-E cell line; the medium was replaced after 10 hours; retroviral supernatant was collected after 48 hours. CD4+ T cells were purified from CD45.1+ CD45.2+ or CD45.2+ SMARTA splenocytes by negative selection (STEMCELL Technologies) and stimulated in 12-well plates pre-coated with 8 μg/mL anti-CD3 (145–2C11; eBioscience) and 8 μg/mL anti-CD28 (37.51; eBioscience) antibodies. After 24 hours, cells were transduced with supernatant containing retrovirus (CD45.1+ CD45.2+ SMARTA with control virus and CD45.2 SMARTA with *Nt5e* shRNAmir virus) in the presence of 8 μg/mL polybrene (MilliporeSigma) by centrifugation for 90 min at 1500 g at 32°C. Twenty-four hours after transduction, AmCyan-positive cells (successfully transduced cells) were sorted, SMARTA cells transduced with the *Nt5e* shRNAmir and control shRNAmir retroviruses were mixed at a 1:1 ratio and a total of 1×10^5 cells were injected into recipient mice through tail vein. After resting for 1 day, recipient mice were infected with 2×10^5 PFU LCMV Armstrong. Mice were sacrificed for cell analysis in spleen, lung and liver 20 days after infection. Lung were digested by collagenase type I (Sigma, Cat#: SCR103) for 1 hour at 37 degree, then crushed and filtered to obtain a single cell suspension. Liver and spleen were directly crushed and filtered into single cells without the enzyme digestion step. Cells were pelleted at a speed of 2000 rpm for 5 min and suspended in 44% Percoll and layered on the top of 67% Percoll. After centrifugation at the speed of 2200 rpm for 22 min, T cell layers were harvested and washed several times before surface marker staining and flow cytometric analysis. All mice were housed in the Stanford Research Animal Facility according to Stanford University guidelines. Animal experiments were approved by the Stanford University Institutional Animal Care and Use Committee.

METHOD DETAILS

Cell culture and flow cytometry—For surface staining, cells were incubated with fluorescence-conjugated antibodies in FACS buffer (2% FBS in PBS) for 30 min at 4°C. Cells were activated with plate-coated anti-CD3/anti-CD28 (BioLegend, OKT3 and CD28.2 clones, Cat#: 317326 and 302934) overnight before staining with anti-CD69 antibody (see STAR methods). For intracellular cytokine assays, cells were stimulated with 50

ng/ml phorbol 12-myristate 13-acetate (PMA, Peprotech, Cat#: 1652981) and 500 ng/ml ionomycin (Peprotech, Cat#: 5608212) in the presence of Brefeldin A (GolgiPlug, from BD Cytofix/Cytoperm plus kit) for 4 hours at 37°C. Cells were then sequentially incubated with surface antibody cocktail, fixed and permeabilized with Cytofix/Cytoperm plus kit (BD Biosciences, Cat#: 555028) and finally stained with fluorescence-labeled antibodies specific to the indicated cytokines. For staining of Ki67, cells were fixed with Cytofix buffer (BD Biosciences) for 10 min at 37°C, followed by permeabilization with pre-chilled Perm buffer III (BD Biosciene) for 30 min on ice, finally stained by Ki67 antibody (see STAR methods) for 45 min at 4°C. Staining for FOXP3, RUNX2 and RUNX3 followed the instruction provided by True-Nuclear Transcription Factor Buffer Set kit (BioLegend, Cat#: 424401). For apoptosis analysis, cells were incubated for the indicated time in the absence or presence of IL-7 (10 ng/ml, Peprotech, Cat#: 200-07) or stem cell factor (20 ng/ml, STEMCELL technologies, Cat#: 78062.1), then stained with fluorescence labeled Annexin V and 7-AAD (BD apoptosis detection kit, Cat#: 559763). For *in vitro* T_{RM} cell differentiation, purified memory T cells were stimulated with anti-CD3/CD28 Dynabeads (ThermoFisher Scientific, Cat#: 11132D; bead to cell ratio 1:2) for 4 days, followed by TGFβ alone or together with IL-15 (TGFβ: 10 ng/ml, STEMCELL Technologies, Cat#: 78067; IL-15: 10 ng/ml, Peprotech, Cat#: 200-15) for 3 more days. Cells were stained with antibody cocktail specific to CXCR6, CD69, CD103 (see STAR methods). For flow-cytometric analysis of cells from human tissues, single-cell suspensions were pre-incubated with Fc Block (BioLegend, Cat#: 422302), stained with fluorochrome-conjugated antibodies and fixed with FOXP3/Transcription Factor Fixation Buffer (Tonbo Biosciences, Cat#: TNB-1020-L050). Tissue-derived cells were gated to exclude dead cells, gate on singlets, followed by gating on CD45^{+}, CD3^{+}, and finally CD4^{+} or CD8^{+} T cells to assess CD45RA, CD73, CD69 and CD103 expression. For tetramer staining, cells were incubated with HLA-A2 tetramers loaded with peptides from EBV BMLF1 280–288: GLCTLVAML or influenza matrix M1 58–66: GILGFVFTL for 1 hour on ice together with or followed by staining for cell surface markers. Tetramers were obtained from the NIH tetramer core facility (Atlanta, GA). Single cell suspensions from mouse spleen, lung and liver were stained with IA[b] LCMV GP66–77 DIYKGVYQFKSV (GP66) and IA[b] LCMV GP61–80 GLKGPDIYKGVYQFKSVEFD (GP61) tetramers, obtained from the NIH tetramer core facility (Emory University, Atlanta, GA), followed by staining with antibodies for cell surface markers (see STAR methods). Dead cells were excluded from the analysis using live/dead fixable aqua (Invitrogen, Cat#: L34966). In adoptive cell transfer experiments, T cells were isolated from mouse lung and spleen and then incubated with antibody cocktail specific to CD45.1, CD45.2, CXCR6, CD69 for surface staining (see STAR methods).

Cells were analyzed on an LSRII or LSR Fortessa (BD Biosciences); flow cytometry data were analyzed using FlowJo (TreeStar) or FCS Express (*De Novo* Software). Cell sorting was done on a FACS Aria2 or Aria3 (BD Biosciences).

Lentiviral transduction of human T cells—RUNX3 cDNA was generating using the primers set hRUNX3_enzy_F: 5′ AACTAGCTAGCatggcatcgaacagcatcttcg 3′ and hRUNX3_enzy_R: 5′ ATACGCGGATCCtcagtagggccgccacac 3′ and cloned into a commercial lentivector containing a GFP reporter gene (pCDH-GFP-Em-CD513B-1 from System

Biosciences). To overexpress RUNX2 in human T cells, we purchased commercial RUNX2/GFP lentivector (Origene, Cat#: RC212884L4). To knockdown RUNX3 or RUNX2 in human T cells, we used RUNX3 or RUNX2 human shRNA plasmid containing GFP reporter gene (Origene, Cat#: TL309682 for RUNX3; Cat#: TL309683 for RUNX2). Lentivirus was produced by transfection of the lentiviral vector, along with psPAX2 (Plasmid #12260; Addgene) and pMD2.G (Plasmid #12259; Addgene) expression vectors into HEK293T cells using Lipofectamine LTX (ThermoFisher Scientific). Lentiviral particles were collected 48 and 72 hours after transfection, filtered through a 0.45 um syringe filter (Millipore), concentrated using Peg-it solution (System Biosciences) and titrated on HEK293T cells. For lentiviral transduction, T cells were activated with anti-CD3/anti-CD28 beads and cultured with a lentiviral vector expressing scrambled control or target plasmids, at a multiplicity of infection of 10 in the presence of 8 mg/ml polybrene (Sigma) and 10 U/ml human IL-2 (Peprotech). After 48 hours, medium was changed once and cells cultured for a total 4 days. Cells were then cultured in medium containing IL-15 and TGFβ for another 3 days for TRM induction.

RNA isolation and quantitative RT-PCR—Total RNA was isolated using either RNeasy Plus Mini or Micro kit (QIAGEN, Cat#: 74134 or 74034), depending on the cell number, and converted to cDNA using High-Capacity cDNA Reverse Transcription Kit (ThermoFisher Scientific, Cat#: 4368813). Quantitative RT-PCR was performed on an Eppendorf Thermal Cycler using Powerup SYBR Green Master Mix (ThermoFisher Scientific, Cat#: A25776) according to the manufacturer's instructions. Expression levels were normalized to ACTB expression and displayed as $2^{-\Delta Ct}*10^{-5}$. Primer sequences are shown in Table S1.

Lymphocyte isolation from human tissues—Tissue samples were maintained in cold saline and brought to the laboratory within 2–4 hours of organ procurement as described (Carpenter et al., 2018; Thome et al., 2014). Spleen samples were chopped up, incubated in enzymatic digest solution (RPMI medium containing 10% FBS, L-glutamate, sodium pyruvate, nonessential amino acids, penicillin-streptomycin, collagenase D [1 mg/ml], trypsin inhibitor [1 mg/ml], and DNase I [50–100 μg/ml]) for 1.5 hours, then mechanically disrupted using a tissue homogenizer (Bullet Blender), filtered through a tissue sieve, and enriched for mononuclear cells using Ficoll density gradient centrifugation. Lung samples were processed as above except for the use of a tissue dissociator (gentleMACS) instead of a homogenizer to mechanically disrupt the samples. Jejunum was separated from intestinal samples after removal of mesenteric lymph nodes. After cleaning off fatty tissue, intestinal tissue segments were washed with PBS and injected with enzymatic digest solution. The segments were then chopped into small pieces and incubated in enzymatic digest solution. After 1.5 hours of incubation, tissue digests were mechanically disrupted using a tissue dissociator (gentleMACS), filtered through a tissue sieve, and enriched for mononuclear cells by density gradient centrifugation using 40% Percoll. The resulting cell suspensions containing high yields of live leukocytes were resuspended in complete RPMI medium.

RNA-seq and data processing—RNA was extracted using RNeasy Plus (QIAGEN, Cat#: 74034) from 300,000 to 500,000 sorted CD73⁻ and CD73⁺CD45RO⁺CD4⁺T cells.

Ribosomal RNA was removed from each RNA extraction using Ribo-Zero Gold rRNA Removal kit (Illumina, Cat#: MRZG12324). RNA-seq libraries were generated by TruSeq Stranded mRNA Library Prep kit (Illumina, Cat#: 20020594) and sequenced on an Illumina HiSeq 4000 sequencer. Sequencing reads were mapped to human genome hg19 using STAR (Dobin et al., 2013). RPKM values were called using HOMER (http://homer.salk.edu/homer/motif/) analyzeRepeats.pl program. Differential expression was performed with DEseq2 using the raw counts of genes associated with each sample generated from HOMER.

Gene set enrichment analysis—Gene expression data from the RNA-seq analysis of $CD73^-$ and $CD73^+CD45RO^+CD4^+T$ cells were compared to *a priori* defined gene sets following standard protocols (https://www.broadinstitute.org/gsea/).

ATAC-Seq library preparation, sequencing, and data preprocessing—50,000 sorted $CD73^-$ and $CD73^+CD45RO^+CD4^+T$ cells were subjected to Omni-ATAC (Corces et al., 2017) to profile the accessible chromatin landscape. ATAC-seq libraries were sequenced on Illumina HiSeq4000 sequencers. ATAC-Seq pair-end reads were trimmed off Illumina adaptor sequences and transposase sequences using a customized script and mapped to hg19 using bowtie (Langmead and Salzberg, 2012) with parameters –S –X2000 –ml. Duplicate reads were discarded with samtools rmdup (Li et al., 2009). Peaks were identified using MACS2 with -f bed -q 0.01–nomodel–shift 0. Overlapped peaks from all samples were merged into a unique peak list, and raw read counts mapped to each peak for each individual sample were quantified. Differentially accessible peaks from the merged union peak list were identified with the edgeR package (Bioconductor) using raw counts of each samples in the union peak list with a fold change threshold of 1.5, and a p value < 0.05.

Transcription factor motif enrichment analysis of differentially accessible sites—Transcriptional factor motifs enriched for selected peak compared to background regions were identified using HOMER "findMotifs-Genome.pl" using default parameters (http://homer.salk.edu/homer/motif/). TF motifs were ranked based on the $-\log_{10}$ (p value) of the enrichment level.

Modeling of transcription factor-regulatory element-target gene networks—We used a previously described inference model of TF-RE-TG regulatory networks (Duren et al., 2017) by integrating RNA-seq, ATAC-seq and human CD4 T cell-specific Trac-looping data (Lai et al., 2018) to assess the network differences in the two memory cell populations. The model quantifies the interaction of each RE with relevant TFs to affect the expression of their TG. We started with an assembled union peak list called from ATAC-seq across all samples as putative REs, identified the upstream TFs and downstream genes for a RE, treated each TF-RE-TG triplet as the basic regulatory unit, ranked them by integrating genomic features, and extracted the significant regulatory relations. RE openness was defined as the fold enrichment of the read starts in this region versus the read starts in a 1M bp background window. Each TF was described by its motif binding score to the RE and its expression level from the RPKM value of RNA-seq. The relationship of a TG with a RE

were derived from the physical interactions measured by the loops called from Trac-looping data (Lai et al., 2018). The computation involves four major steps.

Step 1: Finding TF-RE-TG triplet—For TF-RE pairs, we used HOMER to scan differentially accessible regions to find all positions with substantial similarity to TF's sequence motif or position weight matrix (PWM) and assemble TF-RE pairs. For RE-TG pairs, we considered both proximal and distal regulation. In each population, we used HOMER to annotate differential peaks with nearest genes and select peaks within 5Kb of TSS to construct the proximal RE-TG regulation pair. As for distal regulation, we introduced Trac-looping data in CD4$^+$ T cells (Lai et al., 2018), selected region-region pairs if either region was located in promoter, and expanded both regions in the pair by 2.5kb into both directions. Then, we overlapped the differential peaks with those selected pairs of Trac-looping data to construct the distal RE-TG regulation pair. We aggregated the two sets of pairs together as the predicted RE-TG sets. Through matching TF-RE pair and RE-TG pair, we constructed all candidate TF-RE-TG triplets in the network.

Step 2: Collecting genomic features from ATAC-seq and RNA-seq data—After identifying all TF-RE-TG triplets, we determined a regulatory score and ranked triplets for both populations. Scores were derived from the following variables in the RNA-seq and ATAC-seq data: differences in TF and TG expression, differences in openness of REs, TF binding derived from motif occurrence.

1. Expression of TF and TG—Gene expression was quantified as RPKM (Reads Per Kilobase of transcript per Million reads mapped). Fold change of total number of reads mapped to TF or TG (M_i) with gene length L_{TF} or L_{TG} to the totally mapped reads N in the experiment,

$$X_{TG} = \frac{M_i / L_{TG}}{N / 10^9} \tag{1}$$

$$X_{TF} = \frac{M_i / L_{TF}}{N / 10^9} \tag{2}$$

Superscript i,j were added to distinguish the expression of TF and TG in sample i and j(X^i_{TF}, X^j_{TF}).

Thus, we obtained the gene expression and calculated its fold change as max {1, average B} / max {1, average A}, where average B and average A are the average expression values in B and A populations. Fold difference over 1 means increase, fold difference below 1 means decrease, and fold differences = 1 means no obvious expression difference (i.e., RPKM 1) detected among all samples.

2. REs' openness—The RE is more likely to be in the open chromatin region if TF utilizes this RE to regulate TG. We defined openness for RE from ATAC-seq. ATAC-seq measures the count of reads in a given region. We quantified the openness for the RE e_i by a fold change score, which computed the enrichment of read counts in e_i by comparing with a

larger background region. Briefly, let N_i be the number of reads in RE e_i of length L_i and G_i that in the W background window around this RE. The openness of RE e_i can be defined as

$$O_i = \frac{N_i/L_i}{G_i/W} \tag{3}$$

3. Motif enrichment score—We used HOMER for motif enrichment analysis on differentially accessible peaks.

We set the $-\log(p\ value)$ of each motif fromHOMER outputs as enrichment score E^i_{TF} which represents the enrichment of TF's corresponding motif in differentially accessible peaks in sample i.

4. TF activity score—We defined TF's activity score TFA_i to represent the activity of TF in sample i, which combines its expression change and corresponding motif's enrichment score. X^r is the TF expression level in reference. It is formally defined as:

$$TFA_i = \frac{X^i_{TF}}{X^r_{TF}} \times E^i_{TF} \tag{4}$$

Step 3: Integrate genomic features and rank TF-RE-TG triples—Our aim was to model how a TF regulated a TG via REs with conditions measurement in matched ATAC-seq and RNA-seq data. For a given TF-RE-TG triplet, we assumed that TF regulated this TG's expression by REs. Thus, we can collect the genomic features for TF-RE-TG triplets in CD73$^+$ and CD73$^-$ cells and calculate the fold change for openness of RE and expression of TF and TG.

With those features, we assumed a normal distribution for each feature across all triplets and independence of transformed features. Using Fisher's method, we combined the features into score S.

$$S = \sum_{i=1}^{4} P_i \tag{5}$$

Where P_i is the $-\log(p\ value)$ for the i-th hypothesis to assess the significance level of feature i. When the p value tends to be small, the test statistic S will be large, which suggests that TF-RE-TG regulation is significant. S follows a chi-square distribution with 2K degrees of freedom, from which a p value for the global hypothesis can be easily obtained, K is the number of features being combined (K = 4 in our case). As a result, all the triplets can be ranked by score S and score S converted into p value.

Step 4: Extracting significant TF-RE-TG triplets into network for visualization—By taking a cutoff p value < 0.05, we predicted a set of TF-RE-TG triplets. Pooling all the triplets together, we then have a TF-RE-TG network, where TF and TG are nodes, and RE is

the edge. We counted the node number for TF and ranked them in each population. TF-TG networks were visualized by Cytoscape (Shannon et al., 2003).

QUANTIFICATION AND STATISTICAL ANALYSIS

Statistical analysis was performed using Prism (GraphPad). Paired or unpaired two-tailed Student's t tests were used for comparing two groups. A two-tailed Pearson's correlation test was used for correlation analysis. One-way ANOVA with Tukey's post hoc test was used for multi-group comparisons. $p < 0.05$ was considered statistically significant.

Supplementary Material

Refer to Web version on PubMed Central for supplementary material.

ACKNOWLEDGMENTS

REFERENCES

Ahmed R, Salmi A, Butler LD, Chiller JM, and Oldstone MB (1984). Selection of genetic variants of lymphocytic choriomeningitis virus in spleens of persistently infected mice. Role in suppression of cytotoxic T lymphocyte response and viral persistence. J. Exp. Med 160, 521–540. [PubMed: 6332167]

Akondy RS, Fitch M, Edupuganti S, Yang S, Kissick HT, Li KW, Youngblood BA, Abdelsamed HA, McGuire DJ, Cohen KW, et al. (2017). Origin and differentiation of human memory CD8 T cells after vaccination. Nature 552, 362–367. [PubMed: 29236685]

Allard B, Longhi MS, Robson SC, and Stagg J (2017). The ectonucleotidases CD39 and CD73: Novel checkpoint inhibitor targets. Immunol. Rev 276, 121–144. [PubMed: 28258700]

Alsuliman A, Muftuoglu M, Khoder A, Ahn YO, Basar R, Verneris MR, Muranski P, Barrett AJ, Liu E, Li L, et al. (2017). A subset of virus-specific CD161$^+$ T cells selectively express the multidrug transporter MDR1 and are resistant to chemotherapy in AML. Blood 129, 740–758. [PubMed: 27821506]

Amezcua Vesely MC, Pallis P, Bielecki P, Low JS, Zhao J, Harman CCD, Kroehling L, Jackson R, Bailis W, Licona-Limón P, et al. (2019). Effector T$_H$17 Cells Give Rise to Long-Lived T$_{RM}$ Cells that Are Essential for an Immediate Response against Bacterial Infection. Cell 178, 1176–1188. [PubMed: 31442406]

Araki K, Morita M, Bederman AG, Konieczny BT, Kissick HT, Sonenberg N, and Ahmed R (2017). Translation is actively regulated during the differentiation of CD8$^+$ effector T cells. Nat. Immunol 18, 1046–1057. [PubMed: 28714979]

Banerjee A, Gordon SM, Intlekofer AM, Paley MA, Mooney EC, Lindsten T, Wherry EJ, and Reiner SL (2010). Cutting edge: The transcription factor eomesodermin enables CD8+ T cells to compete for the memory cell niche. J. Immunol 185, 4988–4992. [PubMed: 20935204]

Böttcher JP, Beyer M, Meissner F, Abdullah Z, Sander J, Höchst B, Eickhoff S, Rieckmann JC, Russo C, Bauer T, et al. (2015). Functional classification of memory CD8(+) T cells by CX3CR1 expression. Nat. Commun 6, 8306. [PubMed: 26404698]

Cao W, Fang F, Gould T, Li X, Kim C, Gustafson C, Lambert S, Weyand CM, and Goronzy JJ (2020). Ecto-NTPDase CD39 is a negative checkpoint that inhibits follicular helper cell generation. J. Clin. Invest 130, 3422–3436. [PubMed: 32452837]

Carpenter DJ, Granot T, Matsuoka N, Senda T, Kumar BV, Thome JJC, Gordon CL, Miron M, Weiner J, Connors T, et al. (2018). Human immunology studies using organ donors: Impact of clinical variations on immune parameters in tissues and circulation. Am. J. Transplant 18, 74–88. [PubMed: 28719147]

Cekic C, and Linden J (2014). Adenosine A2A receptors intrinsically regulate CD8+ T cells in the tumor microenvironment. Cancer Res. 74, 7239–7249. [PubMed: 25341542]

Corces MR, Trevino AE, Hamilton EG, Greenside PG, Sinnott-Armstrong NA, Vesuna S, Satpathy AT, Rubin AJ, Montine KS, Wu B, et al. (2017). An improved ATAC-seq protocol reduces background and enables interrogation of frozen tissues. Nat. Methods 14, 959–962. [PubMed: 28846090]

De Boer RJ, and Perelson AS (2013). Quantifying T lymphocyte turnover. J. Theor. Biol 327, 45–87. [PubMed: 23313150]

Dobin A, Davis CA, Schlesinger F, Drenkow J, Zaleski C, Jha S, Batut P, Chaisson M, and Gingeras TR (2013). STAR: ultrafast universal RNA-seq aligner. Bioinformatics 29, 15–21. [PubMed: 23104886]

Duhen T, Ni C, and Campbell D (2014). Identification of a specific gene signature in human Th1/17 cells (BA13P.126). J. Immunol 192, 177.12.

Duren Z, Chen X, Jiang R, Wang Y, and Wong WH (2017). Modeling gene regulation from paired expression and chromatin accessibility data. Proc. Natl. Acad. Sci. USA 114, E4914–E4923. [PubMed: 28576882]

Ely KH, Cookenham T, Roberts AD, and Woodland DL (2006). Memory T cell populations in the lung airways are maintained by continual recruitment. J. Immunol 176, 537–543. [PubMed: 16365448]

Enamorado M, Iborra S, Priego E, Cueto FJ, Quintana JA, Martínez-Cano S, Mejías-Pérez E, Esteban M, Melero I, Hidalgo A, and Sancho D (2017). Enhanced anti-tumour immunity requires the interplay between resident and circulating memory CD8+ T cells. Nat. Commun 8, 16073. [PubMed: 28714465]

Fang F, Yu M, Cavanagh MM, Hutter Saunders J, Qi Q, Ye Z, Le Saux S, Sultan W, Turgano E, Dekker CL, et al. (2016). Expression of CD39 on Activated T Cells Impairs their Survival in Older Individuals. Cell Rep. 14, 1218–1231. [PubMed: 26832412]

Gattinoni L, Zhong XS, Palmer DC, Ji Y, Hinrichs CS, Yu Z, Wrzesinski C, Boni A, Cassard L, Garvin LM, et al. (2009). Wnt signaling arrests effector T cell differentiation and generates CD8+ memory stem cells. Nat. Med 15, 808–813. [PubMed: 19525962]

Gerlach C, Moseman EA, Loughhead SM, Alvarez D, Zwijnenburg AJ, Waanders L, Garg R, de la Torre JC, and von Andrian UH (2016). The Chemokine Receptor CX3CR1 Defines Three Antigen-Experienced CD8 T Cell Subsets with Distinct Roles in Immune Surveillance and Homeostasis. Immunity 45, 1270–1284. [PubMed: 27939671]

Gossel G, Hogan T, Cownden D, Seddon B, and Yates AJ (2017). Memory CD4 T cell subsets are kinetically heterogeneous and replenished from naive T cells at high levels. eLife 6, e23013. [PubMed: 28282024]

Graham SM, Vass JK, Holyoake TL, and Graham GJ (2007). Transcriptional analysis of quiescent and proliferating CD34+ human hemopoietic cells from normal and chronic myeloid leukemia sources. Stem Cells 25, 3111–3120. [PubMed: 17717066]

Haluszczak C, Akue AD, Hamilton SE, Johnson LD, Pujanauski L, Teodorovic L, Jameson SC, and Kedl RM (2009). The antigen-specific CD8+ T cell repertoire in unimmunized mice includes memory phenotype cells bearing markers of homeostatic expansion. J. Exp. Med 206, 435–448. [PubMed: 19188498]

Himer L, Csóka B, Selmeczy Z, Koscsó B, Pócza T, Pacher P, Németh ZH, Deitch EA, Vizi ES, Cronstein BN, and Haskó G (2010). Adenosine A2A receptor activation protects CD4+

T lymphocytes against activation-induced cell death. FASEB J. 24, 2631–2640. [PubMed: 20371613]

Hirata Y, Furuhashi K, Ishii H, Li HW, Pinho S, Ding L, Robson SC, Frenette PS, and Fujisaki J (2018). CD150^high Bone Marrow Tregs Maintain Hematopoietic Stem Cell Quiescence and Immune Privilege via Adenosine. Cell Stem Cell 22, 445–453. [PubMed: 29456159]

Hu G, and Chen J (2013). A genome-wide regulatory network identifies key transcription factors for memory CD8+ T-cell development. Nat. Commun 4, 2830. [PubMed: 24335726]

Iwata M, Hirakiyama A, Eshima Y, Kagechika H, Kato C, and Song SY (2004). Retinoic acid imprints gut-homing specificity on T cells. Immunity 21, 527–538. [PubMed: 15485630]

Jameson SC, and Masopust D (2009). Diversity in T cell memory: an embarrassment of riches. Immunity 31, 859–871. [PubMed: 20064446]

Jameson SC, and Masopust D (2018). Understanding Subset Diversity in T Cell Memory. Immunity 48, 214–226. [PubMed: 29466754]

Kawabe T, Jankovic D, Kawabe S, Huang Y, Lee PH, Yamane H, Zhu J, Sher A, Germain RN, and Paul WE (2017). Memory-phenotype CD4+ T cells spontaneously generated under steady-state conditions exert innate T_H1-like effector function. Sci. Immunol 2, 12.

Kim CH, Kunkel EJ, Boisvert J, Johnston B, Campbell JJ, Genovese MC, Greenberg HB, and Butcher EC (2001). Bonzo/CXCR6 expression defines type 1-polarized T-cell subsets with extralymphoid tissue homing potential. J. Clin. Invest 107, 595–601. [PubMed: 11238560]

Koutsakos M, Illing PT, Nguyen THO, Mifsud NA, Crawford JC, Rizzetto S, Eltahla AA, Clemens EB, Sant S, Chua BY, et al. (2019). Human CD8+ T cell cross-reactivity across influenza A, B and C viruses. Nat. Immunol 20, 613–625. [PubMed: 30778243]

Kumar BV, Ma W, Miron M, Granot T, Guyer RS, Carpenter DJ, Senda T, Sun X, Ho SH, Lerner H, et al. (2017). Human Tissue-Resident Memory T Cells Are Defined by Core Transcriptional and Functional Signatures in Lymphoid and Mucosal Sites. Cell Rep. 20, 2921–2934. [PubMed: 28930685]

Lai B, Tang Q, Jin W, Hu G, Wangsa D, Cui K, Stanton BZ, Ren G, Ding Y, Zhao M, et al. (2018). Trac-looping measures genome structure and chromatin accessibility. Nat. Methods 15, 741–747. [PubMed: 30150754]

Langmead B, and Salzberg SL (2012). Fast gapped-read alignment with Bowtie 2. Nat. Methods 9, 357–359. [PubMed: 22388286]

Lee JY, Hamilton SE, Akue AD, Hogquist KA, and Jameson SC (2013). Virtual memory CD8 T cells display unique functional properties. Proc. Natl. Acad. Sci. USA 110, 13498–13503. [PubMed: 23898211]

Li H, Handsaker B, Wysoker A, Fennell T, Ruan J, Homer N, Marth G, Abecasis G, and Durbin R; 1000 Genome Project Data Processing Sub-group (2009). The Sequence Alignment/Map format and SAMtools. Bioinformatics 25, 2078–2079. [PubMed: 19505943]

Li C, Zhu B, Son YM, Wang Z, Jiang L, Xiang M, Ye Z, Beckermann KE, Wu Y, Jenkins JW, et al. (2019). The Transcription Factor Bhlhe40 Programs Mitochondrial Regulation of Resident CD8+ T Cell Fitness and Functionality. Immunity 51, 491–507. [PubMed: 31533057]

Mackay LK, Minnich M, Kragten NA, Liao Y, Nota B, Seillet C, Zaid A, Man K, Preston S, Freestone D, et al. (2016). Hobit and Blimp1 instruct a universal transcriptional program of tissue residency in lymphocytes. Science 352, 459–463. [PubMed: 27102484]

Miller CH, Klawon DEJ, Zeng S, Lee V, Socci ND, and Savage PA (2020). Eomes identifies thymic precursors of self-specific memory-phenotype CD8+ T cells. Nat. Immunol 21, 567–577. [PubMed: 32284593]

Milner JJ, and Goldrath AW (2018). Transcriptional programming of tissue-resident memory CD8+ T cells. Curr. Opin. Immunol 51, 162–169. [PubMed: 29621697]

Milner JJ, Toma C, Yu B, Zhang K, Omilusik K, Phan AT, Wang D, Getzler AJ, Nguyen T, Crotty S, et al. (2017). Runx3 programs CD8+ T cell residency in non-lymphoid tissues and tumours. Nature 552, 253–257. [PubMed: 29211713]

Murata K, Tsukahara T, Emori M, Shibayama Y, Mizushima E, Matsumiya H, Yamashita K, Kaya M, Hirohashi Y, Kanaseki T, et al. (2016). Identification of a novel human memory T-cell population

with the characteristics of stem-like chemo-resistance. OncoImmunology 5, e1165376. [PubMed: 27471640]

Olesin E, Nayar R, Saikumar-Lakshmi P, and Berg LJ (2018). The Transcription Factor Runx2 Is Required for Long-Term Persistence of Antiviral CD8+ Memory T Cells. Immunohorizons 2, 251–261. [PubMed: 30264035]

Olive AJ, Gondek DC, and Starnbach MN (2011). CXCR3 and CCR5 are both required for T cell-mediated protection against C. trachomatis infection in the murine genital mucosa. Mucosal Immunol. 4, 208–216. [PubMed: 20844481]

Park SL, and Mackay LK (2019). Bhlhe40 Keeps Resident T Cells Too Fit to Quit. Immunity 51, 418–420. [PubMed: 31533052]

Purton JF, Tan JT, Rubinstein MP, Kim DM, Sprent J, and Surh CD (2007). Antiviral CD4+ memory T cells are IL-15 dependent. J. Exp. Med 204, 951–961. [PubMed: 17420265]

Quinn KM, Fox A, Harland KL, Russ BE, Li J, Nguyen THO, Loh L, Olshanksy M, Naeem H, Tsyganov K, et al. (2018). Age-Related Decline in Primary CD8+ T Cell Responses Is Associated with the Development of Senescence in Virtual Memory CD8+ T Cells. Cell Rep. 23, 3512–3524. [PubMed: 29924995]

Reis BS, Rogoz A, Costa-Pinto FA, Taniuchi I, and Mucida D (2013). Mutual expression of the transcription factors Runx3 and ThPOK regulates intestinal CD4+ T cell immunity. Nat. Immunol 14, 271–280. [PubMed: 23334789]

Rittiner JE, Korboukh I, Hull-Ryde EA, Jin J, Janzen WP, Frye SV, and Zylka MJ (2012). AMP is an adenosine A1 receptor agonist. J. Biol. Chem 287, 5301–5309. [PubMed: 22215671]

Rosemblatt MV, Parra-Tello B, Briceño P, Rivas-Yáñez E, Tucer S, Saavedra-Almarza J, Hörmann P, Martínez BA, Lladser Á, Rosemblatt M, et al. (2021). Ecto-5′-Nucleotidase (CD73) Regulates the Survival of CD8+ T Cells. Front. Cell Dev. Biol 9, 647058, 647058. [PubMed: 33928082]

Sadaoka T, and Mori Y (2018). Vaccine Development for Varicella-Zoster Virus. Adv. Exp. Med. Biol 1045, 123–142. [PubMed: 29896666]

Saze Z, Schuler PJ, Hong CS, Cheng D, Jackson EK, and Whiteside TL (2013). Adenosine production by human B cells and B cell-mediated suppression of activated T cells. Blood 122, 9–18. [PubMed: 23678003]

Schenkel JM, and Masopust D (2014). Tissue-resident memory T cells. Immunity 41, 886–897. [PubMed: 25526304]

Seddon B, Tomlinson P, and Zamoyska R (2003). Interleukin 7 and T cell receptor signals regulate homeostasis of CD4 memory cells. Nat. Immunol 4, 680–686. [PubMed: 12808452]

Shannon P, Markiel A, Ozier O, Baliga NS, Wang JT, Ramage D, Amin N, Schwikowski B, and Ideker T (2003). Cytoscape: a software environment for integrated models of biomolecular interaction networks. Genome Res. 13, 2498–2504. [PubMed: 14597658]

Slütter B, Van Braeckel-Budimir N, Abboud G, Varga SM, Salek-Ardakani S, and Harty JT (2017). Dynamics of influenza-induced lung-resident memory T cells underlie waning heterosubtypic immunity. Sci. Immunol 2, eaag2031. [PubMed: 28783666]

Sosinowski T, White JT, Cross EW, Haluszczak C, Marrack P, Gapin L, and Kedl RM (2013). CD8α+ dendritic cell trans presentation of IL-15 to naive CD8+ T cells produces antigen-inexperienced T cells in the periphery with memory phenotype and function. J. Immunol 190, 1936–1947. [PubMed: 23355737]

Surh CD, and Sprent J (2008). Homeostasis of naive and memory T cells. Immunity 29, 848–862. [PubMed: 19100699]

Thome JJ, Yudanin N, Ohmura Y, Kubota M, Grinshpun B, Sathaliyawala T, Kato T, Lerner H, Shen Y, and Farber DL (2014). Spatial map of human T cell compartmentalization and maintenance over decades of life. Cell 159, 814–828. [PubMed: 25417158]

Tian Y, Babor M, Lane J, Schulten V, Patil VS, Seumois G, Rosales SL, Fu Z, Picarda G, Burel J, et al. (2017). Unique phenotypes and clonal expansions of human CD4 effector memory T cells re-expressing CD45RA. Nat. Commun 8, 1473. [PubMed: 29133794]

Wang C, Kang SG, Lee J, Sun Z, and Kim CH (2009). The roles of CCR6 in migration of Th17 cells and regulation of effector T-cell balance in the gut. Mucosal Immunol. 2, 173–183. [PubMed: 19129757]

Weng NP, Araki Y, and Subedi K (2012). The molecular basis of the memory T cell response: differential gene expression and its epigenetic regulation. Nat. Rev. Immunol 12, 306–315. [PubMed: 22421787]

White JT, Cross EW, Burchill MA, Danhorn T, McCarter MD, Rosen HR, O'Connor B, and Kedl RM (2016). Virtual memory T cells develop and mediate bystander protective immunity in an IL-15-dependent manner. Nat. Commun 7, 11291. [PubMed: 27097762]

White JT, Cross EW, and Kedl RM (2017). Antigen-inexperienced memory CD8$^+$ T cells: where they come from and why we need them. Nat. Rev. Immunol 17, 391–400. [PubMed: 28480897]

Younes SA, Punkosdy G, Caucheteux S, Chen T, Grossman Z, and Paul WE (2011). Memory phenotype CD4 T cells undergoing rapid, nonburst-like, cytokine-driven proliferation can be distinguished from antigen-experienced memory cells. PLoS Biol. 9, e1001171. [PubMed: 22022231]

Zhang N, and Bevan MJ (2013). Transforming growth factor-β signaling controls the formation and maintenance of gut-resident memory T cells by regulating migration and retention. Immunity 39, 687–696. [PubMed: 24076049]

Highlights

- CD73 defines subsets of memory T cells distinct from previous classifications

- CD73$^+$ and CD73$^-$ T cells are governed by distinct transcriptional factor networks

- CD73$^+$ T cells are long-lived memory cells that can differentiate into T$_{RM}$ cells

- Decline in CD73$^+$ T cells may account for defective immune memory with age
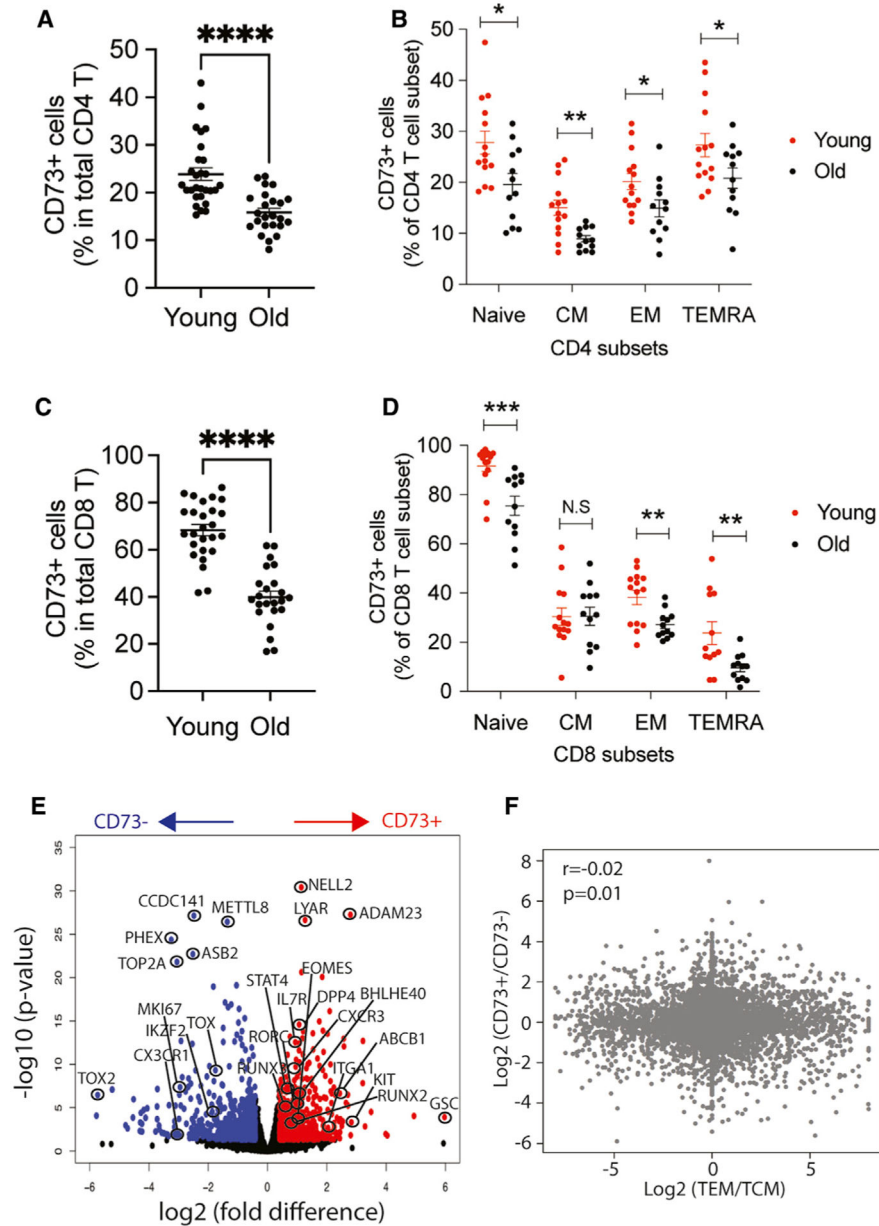
Figure 1. Expression of CD73 identifies a memory T cell subset that is distinct from conventional subsets and that decreases with age

(A–D) Frequencies of CD73$^+$ cells in total peripheral CD4 (A) and CD8 (C) T cells from 28 young (<35 years) and 24 older (>65 years) individuals and in subsets of CD4 (B) and CD8 cells (D) from 14 young (<35 years, red) and 12 older (>65 years, black) individuals. Results are shown as dot plots of frequencies with means as indicated. Frequencies in T cells from young and old adults were compared by unpaired t test; *p < 0.05, **p < 0.01, ***p < 0.001, ****p < 0.0001, N.S., not significant.

(E) Volcano plot of genes differentially expressed in CD73$^+$ and CD73$^-$ memory CD4 T cells. Genes significantly (p < 0.05) higher (red) or lower (blue) in expression (by >30%) in CD73$^+$ T cells are indicated by color. Selected genes of immunological relevance are labeled.

(F) Transcriptomes of CD73$^+$ and CD73$^-$ memory CD4 T cells and conventional T$_{CM}$ and T$_{EM}$ (from GEO: GSE97863 [Tian et al., 2017]) are compared. Results are shown as the fold difference between T$_{CM}$ and T$_{EM}$ plotted versus the fold difference between CD73$^+$ and CD73$^-$ memory CD4 T cells. Correlation coefficient and p value were calculated based on Pearson's product-moment correlation analysis.

See also Figure S1.

Figure 2. Distinctive features of the transcriptome of CD73$^+$ memory CD4 T cells

(A) Genes overexpressed by CD73$^+$ T cells were analyzed for functional enrichment using the DAVID Bioinformatics Tool. Genes from selected enriched gene ontology terms (p < 0.001) are shown as heat maps.

(B) Gene set enrichment analysis (GSEA) of transcriptome data showed a correlation for CD73$^+$ cells with Hallmark_Inflammatory response and KEG-G_Ribosome.

(C) Purified CD73$^+$ and CD73$^−$ memory CD4 T cells were activated by plate-immobilized anti-CD3/CD28 Abs; CD69 cell-surface expression was determined after 12 h.

(D and E) Memory CD4 (D) and CD8 (E) T cells were stimulated with PMA/ionomycin for 3–4 h before intracellular cytokine staining. Results are shown as the frequencies of cells

producing indicated cytokines. MFIs of cytokine expression are shown in Figures S1D and S1E.

(F) Data were analyzed for the co-expression of IL-2, TNF-α, and IFN-γ for CD4 T cells and IL-2, granzyme B, and IFN-γ for CD8 T cells. Results are shown as representative contour plots and boxplots of the percentage of polyfunctional T cells in the CD73+ (red) and CD73− (black) subsets. Data were compared by two-tailed paired t test.
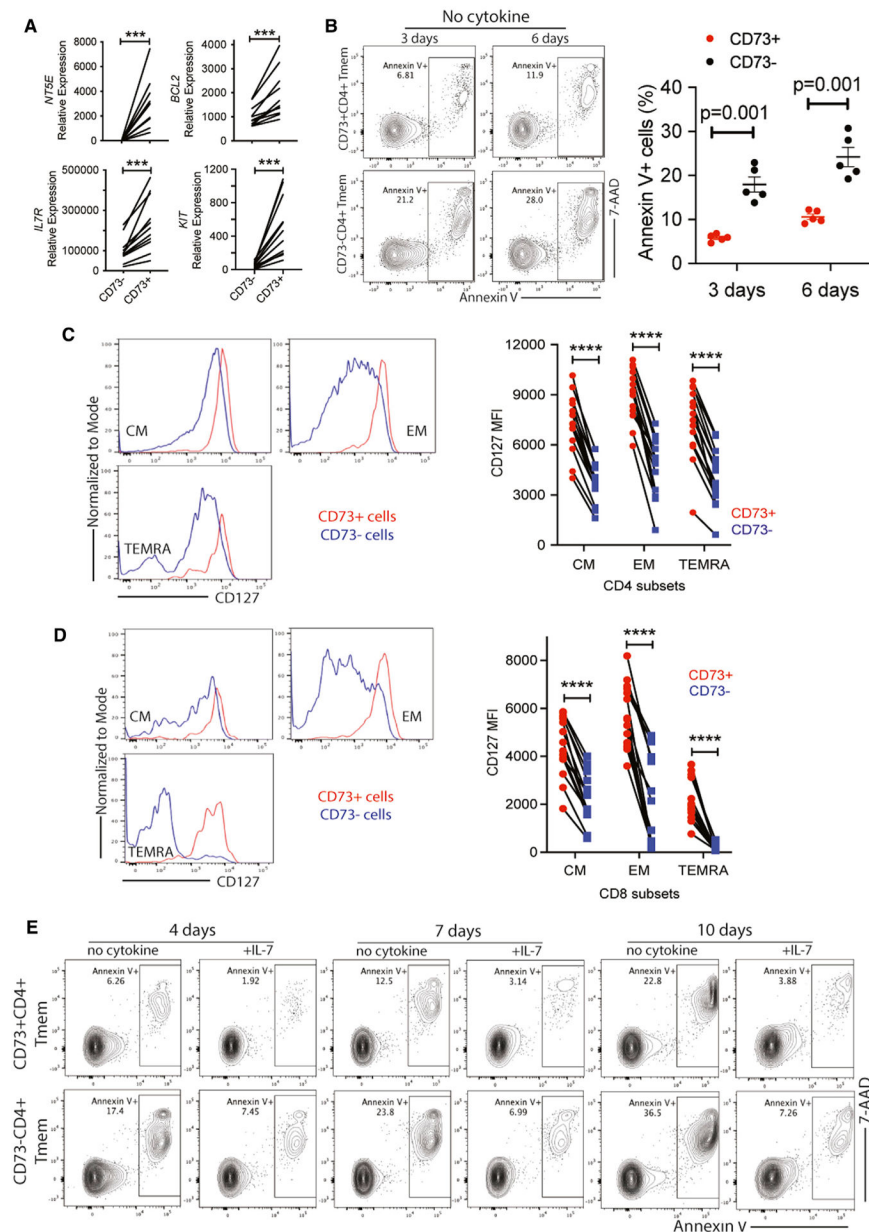
See also Figure S2.

Figure 3. Increased longevity of CD73+ memory T cells

(A) *NT5E*, *BCL2*, *IL7R*, and *KIT* expression quantified by RT-PCR. Data are shown as $2^{(-\text{delta Ct})} * 10^{-5}$.

(B) CD73+ and CD73− memory CD4 T cells, respectively, were cultured in the absence of cytokines. Cells were stained with Annexin V and 7-AAD. Results are shown as representative contour plots (left) and summary data (right).

(C and D) CD127 (IL-7R) expression on CD73+ versus CD73− cells of CD4 (C) and CD8

(D) memory T cell subsets. Representative histograms (left) and summary data (right).

(E) Cells were cultured in the presence or absence of IL-7 (10 ng/mL) for indicated times and stained with Annexin V and 7-AAD. Contour plots are representative of four experiments.

Data were compared by two-tailed paired t test. ***p < 0.001, ****p < 0.0001.
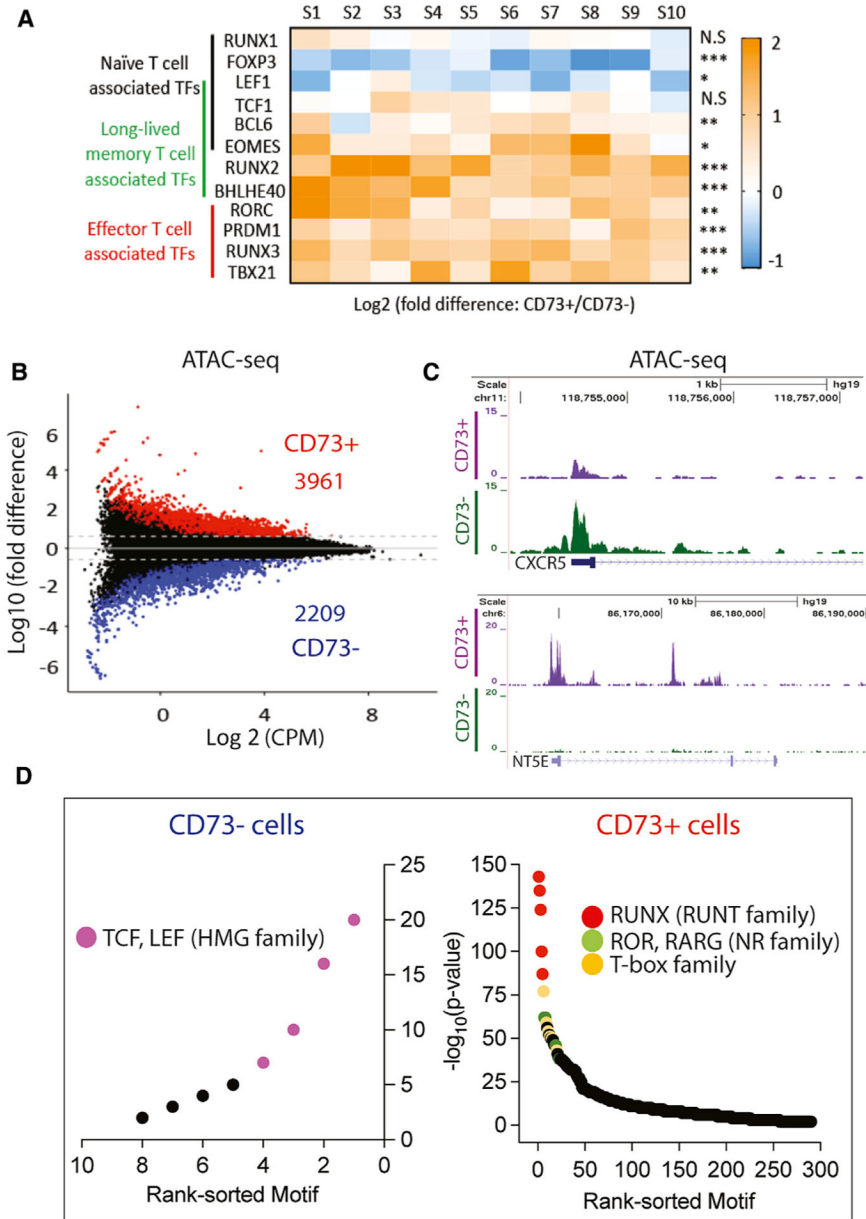See also Figure S3.

Figure 4. Differential chromatin accessibilities in CD73+ and CD73− memory T cells

(A) Expression profile of 12 T cell-related transcriptional factors in CD73+ versus CD73− memory CD4 T cells from 10 healthy individuals (S1 to S10) as determined by RT-PCR. Data were compared by two-tailed paired t test. *p < 0.05, **p < 0.01, ***p < 0.001, N.S., not significant.

(B) Chromatin accessibility in CD73+ and CD73− memory CD4 T cells from three healthy individuals determined by ATAC-seq. Results are shown as MA plot with differentially accessible sites (1.5-fold difference, p < 0.05) indicated by red (more open in CD73+ cells) and blue (more open in CD73− cells). CPM, count per million reads.

(C) Chromatin accessibility tracks across the genes *NT5E* encoding CD73 and *CXCR5* in CD73+ (purple) and CD73− (green) memory T cells.

(D) TF motif enrichment at sites with decreased (left) and increased accessibility (right) in CD73$^+$ versus CD73$^-$ cells. Colors indicate TF families with shared motifs.
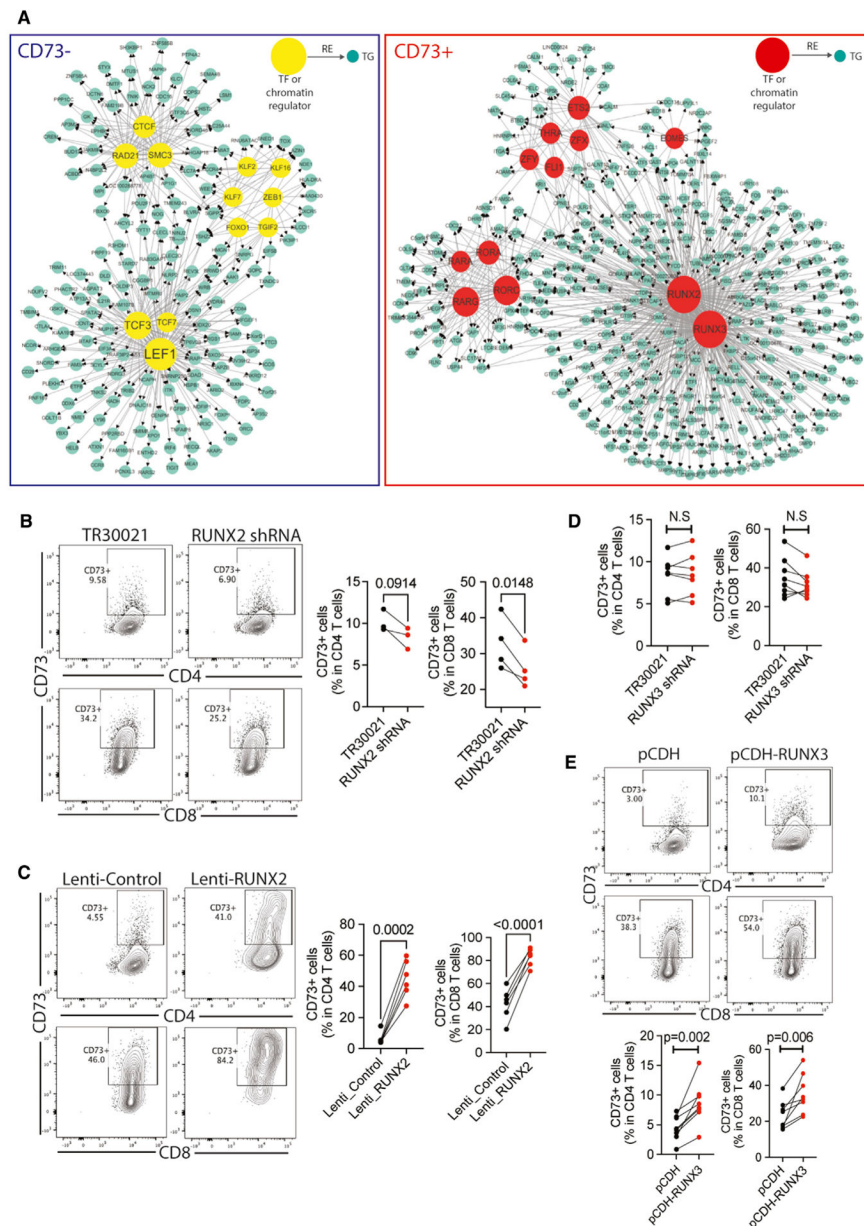
Figure 5. CD73$^+$ and CD73$^-$ memory T cells are governed by distinct transcription factor networks

(A) Transcription factor-regulatory element-target gene (TF-RE-TG) networks in CD73$^-$ (left) or CD73$^+$ cells (right) were modeled as described in Figure S3. Red and yellow nodes represent transcriptional factors (TFs) or chromatin regulators (CRs); the green nodes represent their target genes (TGs) that are differentially expressed in CD73$^+$ and CD73$^-$ memory T cells. The size of TF nodes corresponds to the number of TF connections. (B–E) Freshly isolated human total T cells were activated and infected with GFP$^+$ lentivirus containing *RUNX2* shRNA (B) *RUNX2* cDNA (C), *RUNX3* shRNA (D), and *RUNX3* cDNA (E) respectively. TR30021, pCDH, and Lenti-Control served as respective controls. Transduced cells were cultured for 7 days, before CD73 expression in gated GFP$^+$ cells were assessed.

Results are compared by two-tailed paired t test. N.S., not significant. See also Figure S5.
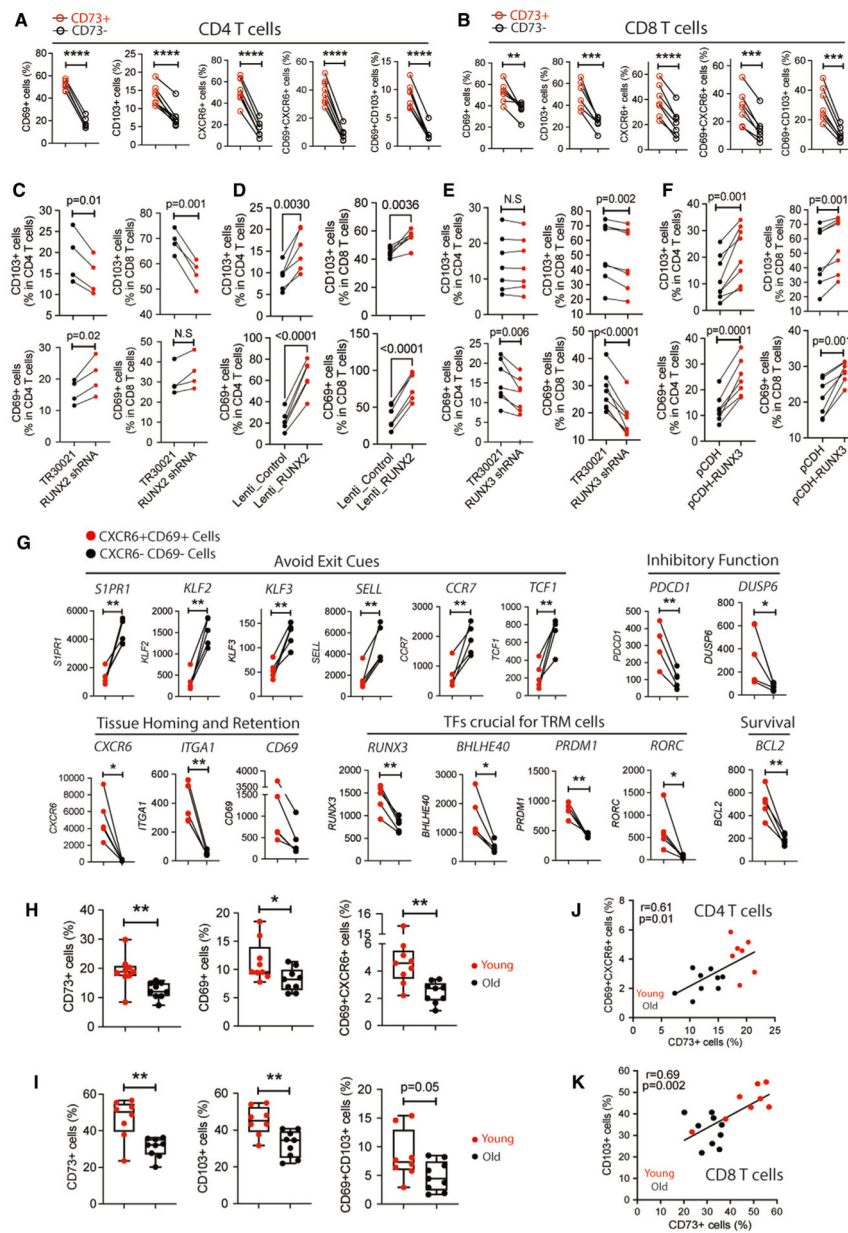
Figure 6. CD73⁺ memory T cells are prone to differentiate into cells with a T_RM phenotype
(A and B) Freshly isolated memory T cells were activated *in vitro* by anti-CD3/CD28 Dynabeads for 4 days followed by culture with TGF-β/IL-15 for 3 days. CD4 (A) and CD8 (B) T cells were analyzed by flow cytometry for the T_RM-associated markers CD69, CXCR6, and CD103 in CD73⁺ and CD73⁻ cells.

(C–F) Freshly isolated human total T cells were activated and infected by GFP⁺ lentivirus containing RUNX2 shRNA (C, TR30021 as a control), *RUNX2* cDNA (D, Lenti-Control as a control), *RUNX3* shRNA (E, TR30021 as a control) or *RUNX3* cDNA (F, pCDH as a control) and differentiated under TRM development conditions for 7 days. GFP⁺ cells were gated and analyzed for CD69 and CD103 expression.

(G) Expression profile of 16 of 19 T_{RM} core genes in the CXCR6$^+$CD69$^+$ and the CXCR6$^-$CD69$^-$ CD4 T cell subsets that have the highest and the lowest CD73 expression, respectively. The remaining three genes (*CX3CR1*, *S1PR5*, and *CRTAM*) were undetectable and are not shown. qPCR results are shown as $2^{(-\text{delta Ct})} *10^{-5}$.

(H–K) Freshly isolated memory CD4 (H/J) and CD8 (I/K) T cells from young (<35 years, red symbol) and older (>65 years, black symbol) individuals were differentiated under 4 days of Dynabeads stimulation and 3 days of TGF-β treatment. Expression of CD73, CD69, CXCR6, and CD103 were analyzed by flow cytometry; results are summarized as boxplots (H and I). Frequencies of CD73$^+$ cells correlated with those of CD69$^+$CXCR6$^+$ cells for CD4 T cells (J) and CD103$^+$ cells for CD8 T cells (K) as determined by Pearson's correlation analysis.

Data were compared by two-tailed paired or unpaired t test. One-way ANOVA was used for multi-group comparisons. *p < 0.05, **p < 0.01, ***p < 0.001, ****p < 0.0001. See also Figures S6 and S7.
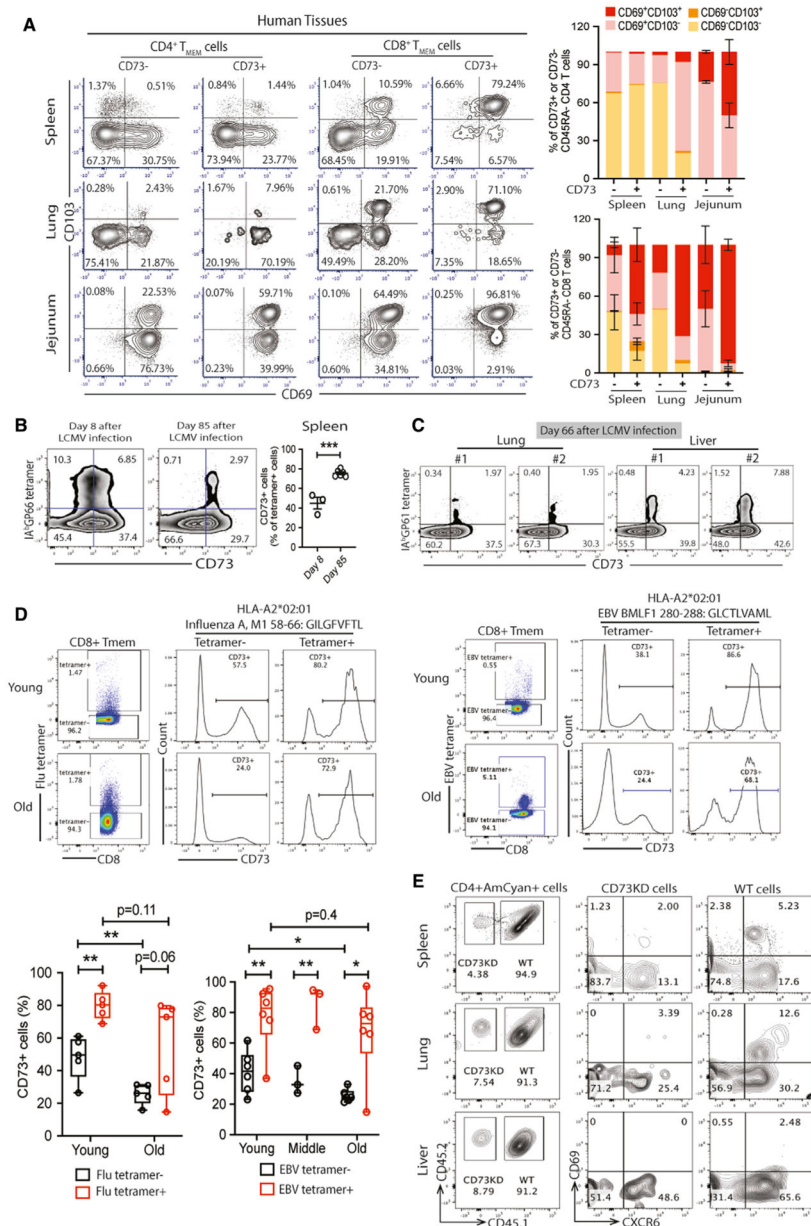
Figure 7. Influence of CD73 on T cell survival and T$_{RM}$ differentiation *in vivo*

(A) Cells isolated from spleen, lung, and jejunum tissues of three organ donors were analyzed for the expression of the TRM markers CD69 and CD103 within CD73$^+$ and CD73-CD45RA$^−$ T cells. Representative contour plots on gated CD45$^+$ cells (left panel for CD4 TMEM cells; right panel for CD8 TMEM cells) are shown. Subset distributions within CD73$^+$ and CD73$^−$ CD45RA$^−$ CD4 and CD8 T cells are summarized as stacked bars. Error bars are included where data from more than one sample were available.

(B) Mice were infected with Armstrong LCMV; CD73 expression on LCMV GP66–77 tetramer$^+$ splenic CD4 T cells was determined on day 8 (effector stage) and day 85 (memory stage). Representative contour plots (left) and summary data from 3–6 mice (right). Data are compared by two-tailed unpaired t test. ***p < 0.001.

(C) CD73 expression on tissue-resident LCMV GP61–80 tetramer[+] CD4 T cells in lung and liver at day 66 after LCMV infection.

(D) CD73 expression on virus-specific CD8 T cells (HLA-A2*02:01 tetramer with GILGFVFTL peptide from influenza M1 protein, left panel; HLA-A2*02:01 tetramer with GLCTLVAML peptide from lytic BMLF1 protein, right panel) from young, middle-age, and old adults. Top panels are representative scatterplots of tetramer staining and histograms of CD73 expression. Bottom panels are summary data of frequencies shown as boxplots. Frequencies in T cells from young and old adults were compared by unpaired t test and frequencies of CD73 expression on tetramer-positive and bulk T cells by paired t test. *$p < 0.05$, **$p < 0.01$. N.S., not significant.

(E) CD4 T cells from WT mice (CD45.2[+]) or heterozygous mice (CD45.1[+]CD45.2[+]) were infected with retrovirus expressing CD73 shRNA or control shRNA. After sorting AmCyan^{+} cells (successfully transduced cells), congenic cells were mixed at 1:1 ratio before being transferred into WT mice through tail vein injection. After 1 day, mice were infected with Armstrong LCMV and sacrificed 20 days after infection. Transferred T cells from spleen, lung, and liver were analyzed for surface markers by flow cytometry. Contour plots are representative of two independent experiments.

KEY RESOURCES TABLE

Reagent or resource	Source	Identifier
Antibodies		
Anti-h CD3 (OKT3)	Biolegend	Cat# 317326; RRID: AB_11150592
Anti-h CD28 (CD28.2)	Biolegend	Cat# 302934; RRID: AB_11148949
Anti-h CD69 (FN50)	Biolegend	Cat# 310904; RRID: AB_314839
Anti-h CD103 (Ber-ACT8)	Biolegend	Cat# 350206; RRID: AB_10641843
Anti-h CXCR6 (K041E5)	Biolegend	Cat# 356010; RRID: AB_2562227
Anti-h CD45 (2D1)	Biolegend	Cat# 368514; RRID: AB_2566374
Anti-h CD45RO (UCHL1)	Biolegend	Cat# 304204; RRID: AB_314420
Anti-h CD45RA (HI100)	Biolegend	Cat# 304134; RRID: AB_2563814
Anti-h CD3 (UCHT1)	Biolegend	Cat# 300424; RRID: AB_493741
Anti-h CD4 (RPA-T4)	Biolegend	Cat# 300506; RRID: AB_314074
Anti-h CD4 (OKT4)	Biolegend	Cat# 317429; RRID: AB_1595438
Anti-h CD8a (RPA-T8)	Biolegend	Cat# 301016; RRID: AB_314134
Anti-h CD62L (DREG-56)	Biolegend	Cat# 304806; RRID: AB_314466
Anti-h CD127 (A019D5)	Biolegend	Cat# 351303; RRID: AB_10719960
Anti-h CD117 (104D2)	Biolegend	Cat# 313203; RRID: AB_314982
Anti-h FOXP3 (206D)	Biolegend	Cat# 320107; RRID: AB_492987
Anti-h IL-2 (MQ1–17H12)	Biolegend	Cat# 500322; RRID: AB_2264650
Anti-h TNFa (MAb11)	Biolegend	Cat# 502916; RRID: AB_493123
Anti-h IL-21 (3A3-N2)	Biolegend	Cat# 513004; RRID: AB_2249025
Anti-h IL-4 (8D4–8)	Biolegend	Cat# 500703; RRID: AB_315115
Anti-h/m Granzyme B (GB11)	Biolegend	Cat# 515406; RRID: AB_2566333
Anti-m CD103 (2E7)	Biolegend	Cat# 121431; RRID: AB_2566551
Anti-m CD186 (SA051D1)	Biolegend	Cat# 151118; RRID: AB_2721669
Anti-m CD73 (TY/11.8)	Biolegend	Cat# 127212; RRID: AB_11219190
Anti-m CD4 (RM4–4)	Biolegend	Cat# 116022; RRID: AB_2715958
Anti-m TCRb chain (H57–597)	Biolegend	Cat# 109207; RRID: AB_313430
Anti-m CD69 (H1.2F3)	Biolegend	Cat# 104522; RRID: AB_2260065
Anti-m CD8a (53–6.7)	Biolegend	Cat# 100706; RRID: AB_312745
Anti-m CD45.1 (A20)	Biolegend	Cat# 110714; RRID: AB_313503
Anti-m CD45.2 (104)	Biolegend	Cat# 109808; RRID: AB_313445
Anti-h CD73 (AD2)	Biolegend	Cat# 562430; RRID: AB_11153119
Anti-h Ki67 (B56)	Biolegend	Cat# 561283; RRID: AB_10716060
Anti-h RUNX3 (R3–5G4)	Biolegend	Cat# 564814; RRID: AB_2738969
Anti-h HLA-A2 (BB7.2)	Biolegend	Cat# 561341; RRID: AB_10646036
Anti-h IFNg (B27)	Biolegend	Cat# 562016; RRID: AB_10894955
Anti-h IL-17A (eBio64DEC17)	ThermoFisher Scientific	Cat# 12-7179-41; RRID: AB_1724138
Anti-m CD3 (145–2C11)	ThermoFisher Scientific	Cat# 14-0031-81; RRID: AB_467048
Anti-m CD28 (37.51)	Abnova	Cat# MAB6206; RRID: AB_10550690
CD45RO microbeads	Miltenyi Biotec	Cat# 130-046-001; RRID: N/A

Reagent or resource	Source	Identifier
Anti-h RUNX2 (D1L7F)	Cell Signaling Technology	Cat# 98059; RRID: AB_2800297
Bacterial and virus strains		
LCMV Armstrong	Laboratory of Rafi Ahmed	(Ahmed et al., 1984)
Biological samples		
Human spleen from 3 organ donors with brain death	LiveOnNY	N/A
Human lung from 3 organ donors with brain death	LiveOnNY	N/A
Human jejunum from 3 organ donors with brain death	LiveOnNY	N/A
Chemicals, peptides, and recombinant proteins		
phorbol 12-myristate 13-acetate	Peprotech	Cat# 1652981
Ionomycin	Peprotech	Cat# 5608212
Human Recombinant IL-2	Peprotech	Cat# 200-02
Human Recombinant IL-7	Peprotech	Cat# 200-07
Human Recombinant IL-15	Peprotech	Cat# 200-15
Human Recombinant TGF-β1	Peprotech	Cat# 100-21
Human Recombinant SCF	STEMCELL Technologies	Cat# 78062.1
HLA-A*02 EBV BMLF1 280–288 (GLCTLVAML) tetramer	NIH Tetramer Core Facility	N/A
HLA-A*02 FLU M1 58–66 (GILGFVFTL) tetramer	NIH Tetramer Core Facility	N/A
IA^b LCMV GP 66–77 (DIYKGVYQFKSV) tetramer	NIH Tetramer Core Facility	N/A
IA^b LCMV GP61–80 (GLKGPDIYKGVYQFKSVEFD) tetramer	NIH Tetramer Core Facility	N/A
Polybrene	Millipore Sigma	Cat# TR-1003-G
Collagenase type I	Millipore Sigma	Cat# SCR103
Collagenase D	Millipore Sigma	Cat# 11088858001
Percoll density gradient media	GE Healthcare Life Sciences	Cat# 17089102
Critical commercial assays		
Fixation/Permeabilization Solution Kit with BD GolgiPlug	BD Biosciences	Cat# 555028
Perm buffer III	BD Biosciences	Cat# 558050
PE Annexin V Apoptosis Detection Kit I	BD Biosciences	Cat# 559763
Human TruStain FcX (Fc Receptor Blocking Solution)	Biolegend	Cat# 422302
True-Nuclear Transcription Factor Buffer Set	Biolegend	Cat# 424401
Foxp3/Transcription Factor Fix/Perm Concentrate (4x)	TONBO Biosciences	Cat# TNB-1020-L050
RosetteSep Human T cell enrichment cocktail	STEMCELL Technologies	Cat# 15061
RosetteSep Human CD4+ T cell enrichment cocktail	STEMCELL Technologies	Cat# 15062
RosetteSep Human CD8+ T cell enrichment cocktail	STEMCELL Technologies	Cat# 15063
EasySep Human Memory CD4+ T cell Enrichment Kit	STEMCELL Technologies	Cat# 19157
EasySep Human Memory CD8+ T cell Enrichment Kit	STEMCELL Technologies	Cat# 19159
Lymphoprep	STEMCELL Technologies	Cat# 07861
EasySep Mouse Naive CD4+ T cell isolation kit	STEMCELL Technologies	Cat# 19765
PEG-it Virus Precipitation Solution	System Biosciences	Cat# LV825A-1
RNeasy Plus Mini Kit	QIAGEN	Cat# 74134
RNeasy Plus Micro Kit	QIAGEN	Cat# 74034
Lipofectamine LTX with PLUS reagent	ThermoFisher Scientific	Cat# 15338100

Reagent or resource	Source	Identifier
High-Capacity cDNA Reverse Transcription Kit	ThermoFisher Scientific	Cat# 4368813
Powerup SYBR Green Master Mix	ThermoFisher Scientific	Cat# A25776
Dynabeads Human T-activator CD3/CD28	ThermoFisher Scientific	Cat# 11132D
Live/dead Fixable Aqua dead cell stain kit	ThermoFisher Scientific	Cat# L34966
Ribo-Zero Gold rRNA Removal kit	Illumina	Cat# MRZG12324
TruSeq Stranded mRNA Library Prep Kit	Illumina	Cat# 20020594
Deposited data		
RNA-seq data of young and old T cell subsets	N/A	SRA: PRJNA638216 (SRA)
RNA-seq data of CD73+ and CD73− CD4+ memory T cells	N/A	GEO: GSE157164 (GEO)
ATAC-seq data of CD73+ and CD73− CD4+ memory T cells	N/A	GEO: GSE157164 (GEO)
Experimental models: Cell lines		
HEK293T cell line	ATCC	Cat# CRL-11268; RRID:CVCL_1926
BHK cell line	ATCC	Cat# 603126/ p632_BHK-21, RRID: CVCL_1915
Vero cell line	ATCC	Cat# 605372/ p622_VERO, RRID: CVCL_0059
Plat-E cell line	ATCC	N/A; RRID: CVCL_B488
Experimental models: Organisms/strains		
C57BL/6J (B6)	Jackson Laboratory	Stock No: 000664
SMARTA TCR transgenic mice	Laboratory of Rafi Ahmed	N/A
Oligonucleotides		
Mouse Nt5e shRNAmir: CAGGTTGAGTTTGATGATAAAG see Table S1 for Q-PCR primers	Laboratory of Jorg J Goronzy	N/A
Recombinant DNA		
pCDH-GFP-Em-CD513B-1 plasmid	System Biosciences	Cat# CD513B-1
psPAX2 plasmid	Addgene	Cat# 12260
pMD2.G plasmid	Addgene	Cat# 12259
RUNX2/GFP lentivector	Origene	Cat# RC212884L4
RUNX2/GFP shRNA plasmid	Origene	TL309683
RUNX3/GFP shRNA plasmid	Origene	TL309682
pLMPd-Amt Vector with Nt5e shRNAmir	Laboratory of Jorg J Goronzy	N/A
Software and algorithms		
FlowJo	TreeStar	RRID: SCR_008520
FCS Express	De Novo Software	RRID: SCR_016431
Prism	GraphPad Software	RRID: SCR_002798
Homer	UCSD	RRID: SCR_010881
GSEA	The Broad Institute	RRID: SCR_003199
DAVID	LHRI	RRID: SCR_001881